LAG3+ CD8+ T cell Subset Drives HR+/HER2- Breast Cancer Reduction in Bispecific Antibody Armed Activated T Cell Therapy

AUTHORS: Robert Weldon Barnes,[*,†] Archana Thakur, [‡] Suna Onengut-Gumuscu,[§] Lawrence G. Lum, [‡,¶] Sepideh Dolatshahi [*,†,¶]

* Department of Biomedical Engineering, University of Virginia (UVA) School of Medicine, Charlottesville, Virginia 22908

[†] University of Virginia Cancer Center, Charlottesville, Virginia, USA

[‡] Division of Hematology & Oncology, Department of Medicine, UVA School of Medicine

[§] Department of Genome Sciences, University of Virginia School of Medicine

[¶] Beirne B. Carter Center for Immunology Research, UVA School of Medicine, Charlottesville, Virginia 22908

RUNNING TITLE: LAG3+ Adoptive T Cells Effectively Reduce HR+ Breast Cancer

CORRESPONDING AUTHOR: Sepideh Dolatshahi, Email: sdolatshahi@virginia.edu, Phone: 434-243-7549

KEYWORDS

Bispecific antibody armed T cell, Checkpoint Inhibitors, Systems Immunology, Therapeutic synergy, Mechanistic Modeling, Rational Design of Combination Therapies, LAG3, TIGIT, HR+/HER2- Breast Cancer.

DECLARATIONS

Availability of data and material – Computational modeling algorithms (OPLS-R) and the mechanistic model of BAT-tumor interactions (ODE model) are available on GitHub (https://github.com/Dolatshahi-Lab). All cytotoxicity and processed flow cytometry data will be provided as Supplemental tables. Raw flow cytometry data and CITE-seq data will be provided upon request.

Competing interests – LGL is cofounder of Transtarget Inc, Founder of BATs, LLC, member of SAB of Rapa Therapeutics and Tundra Targeted Therapeutics and consults for iCell Gene Therapeutics. AT is a cofounder of Alpha Immune LLC.

Funding – This work was funded by SD startup funds, UVA Cancer Center Support Grant P30 CA044579 and LGL UVA startup funds. The UVA Comprehensive Cancer Center Support Grant (P30CA044579) from the NCI additionally supported work performed by the Genome Analysis and Technology Core, RRID:SCR_018883 and Biorepository and Tissue Research Facility, RRID:SCR_022971. This research was also supported by the UVA Farrow Fellowship.

Authors contributions – RWB, SD, and LGL were responsible for the conceptualization of the project and methodologies. RWB and SD wrote the manuscript with input from all authors. SD and LGL provided supervision. RWB performed experiments, analyzed data, and built the computational models. RWB, AT, SOG, LGL, and SD contributed to the design and development of the investigation. SD was responsible for funding acquisition. All authors approved the final version of the manuscript.

Acknowledgements – This work was presented at the 2024 Society for Immunotherapy of Cancer (SITC) annual meeting (Abstract #718). We thank the Dolatshahi lab members and Dr. Kristin Anderson for providing feedback.

Authors' information (optional) –

Robert W. Barnes– ORCID iD 0000-0001-6494-4033

Sepideh Dolatshahi – ORCID iD 0000-0003-0226-0933

Suna Onengut-Gumuscu – ORCID iD 0000-0002-6563-8334

Archana Thakur – ORCID iD 0000-0003-3876-9555

Lawrence G. Lum – ORCID iD 0000-0001-7561-6035

LIST OF ABBREVIATIONS – Tumor microenvironment, TME; Bispecific antibody armed T cell, BATs; checkpoint inhibitor, CPI; hormone receptor-positive, HR+; Lymphocyte activation gene 3, LAG3; Programmed Cell Death Protein 1, PD-1; T cell immunoreceptor with immunoglobulin and ITIM domain, TIGIT; bispecific antibodies, BiAb; overall survival, OS; metastatic breast cancer, MBC; ordinary differential equation, ODE; unarmed activated T cells, ATC; cellular indexing of transcriptomes and epitopes, CITE-seq; real-time cell analysis, RTCA; orthogonalized partial least squares regression, OPLS-R; variable importance in projection, VIP; uniform manifold approximation and projection, UMAP; T cell receptor, TCR.

What is already known on this topic – Bispecific antibody armed T cell (BATs) therapies are adoptive T cell therapies that can effectively reroute T cell cytotoxicity toward cancerous cells, but lack consistent and durable anti-tumor responses. Checkpoint proteins expressed on the surface of activated T cells dampen immune responses and can be overstimulated in solid tumors to hamper tumor clearance by T cells. Checkpoint inhibitor drugs can improve T cell anti-tumor response by blocking checkpoint protein signaling but are only effective if the targeted checkpoint protein is expressed on the T cell and activated in the tumor microenvironment, highlighting an opportunity to enhance BAT efficacy by combining treatment with synergistic CPI.

What this study adds – This study characterizes dynamic, time-resolved patterns in checkpoint protein expression by breast cancer-targeting adoptive T cells and predicts the significance of high-prevalence checkpoint proteins on T cell function. It also demonstrates the use of multivariate statistic and mathematical modeling toward rational design of targets and timing strategies for synergistic combination therapies.

How this study might affect research, practice, or policy – The output of this study provides justification for therapeutic strategies combining adoptive T cell therapies with checkpoint inhibitor drugs targeting TIGIT and LAG3 as a means of improving patient responses in HER2-/HR+ breast cancers.

ABSTRACT

Tumor clearance by T cells is impaired by insufficient tumor antigen recognition, insufficient tumor infiltration, and the immunosuppressive tumor microenvironment (TME). Although targeted T cell therapy circumvents failures in tumor antigen recognition, suppression by the TME and failure to infiltrate the tumor can hinder tumor clearance. Checkpoint inhibitors (CPI) promise to reverse T cell suppression and can be combined with bispecific antibody armed T cell (BATs) therapy to improve clinical outcomes. We hypothesize that adoptively transferred T cell function may be improved by the addition of CPI if the inhibitory pathway is functionally active. This study develops a kinetic-dynamic model of killing of hormone receptor-positive (HR+) breast cancer cells mediated by BATs using single-cell transcriptomic and temporal protein data to identify T cell phenotypes and quantify inhibitory receptor expression. LAG3, PD-1, and TIGIT were

99 identified as inhibitory receptors expressed by cytotoxic effector CD8 BATs upon
100 exposure to HR+ breast cancer cell lines. These data were combined with real-time tumor
101 cytotoxicity data in a multivariate statistical analysis framework to predict the relevant
102 contributions of T cells expressing each receptor to tumor reduction. A mechanistic
103 kinetic-dynamic mathematical model was developed and parametrized using protein
104 expression and cytotoxicity data for in silico validation of the findings of the multivariate
105 statistical analysis. The model corroborated the predictions of the multivariate statistical
106 analysis which identified LAG3+ BATs as the primary effectors, while TIGIT expression
107 dampened cytotoxic function. These results inform CPI selection for BATs combination
108 therapy and provide a framework to maximize BATs anti-tumor function.
109

110 **INTRODUCTION**

111 HR+/HER2- breast cancers represent 68% of all breast cancer diagnoses(1).
112 Targeted adoptive T cell therapies offer an effective approach to elicit T cell immune
113 responses against tumors lacking a sufficiently recognizable tumor antigen(2–6).
114 Bispecific antibody-armed activated T-cell (BATs) therapies utilize activated T cells armed
115 with bispecific antibodies (BiAb) targeting CD3 and a tumor antigen to redirect non-MHC
116 restricted T cell cytotoxicity toward high and low antigen expressing cancer cells(6, 7).
117 This strategy has shown encouraging results in reducing tumor burden, improving quality
118 of life, and improving median overall survival (OS) in patients with stage IV breast(8, 9),
119 prostate(10), and pancreatic(5) cancers and neuroblastoma(11).

120 In a phase I trial involving 17 heavily pretreated HER2-/HR+ metastatic breast
121 cancer (MBC) patients, HER2 BATs therapy achieved a median OS of 27.4 months with

122 59% patients exhibiting stable disease at 14.5 weeks(12). Similarly, a phase II trial with
123 24 HER2-/HR+ MBC patients reported a decrease in tumor markers in 56.5% of patients
124 and a median OS of 15.2 months following HER2 BATs infusions(13). Despite these
125 successes, the lack of consistent and durable anti-tumor responses highlights an
126 opportunity to enhance BAT efficacy by combining treatment with synergistic T cell
127 targeting therapies.

128 Checkpoint inhibitors improve T cell function against solid tumors by preventing
129 inhibitory signaling. While CPIs have shown efficacy in some breast cancers, response
130 rates in HER2-/HR+ patients remain disappointingly low (5-12%) compared to HER2+ or
131 TNBC patients(14–16). CPI efficacy depends on the presence of the target protein and
132 its complimentary ligands or receptors, suggesting that identifying reliable CPI targets in
133 HER2-/HR+ tumors could improve therapeutic outcomes (17, 18). By characterizing
134 inhibitory receptor expression dynamics and BATs function, this study investigates
135 whether the timing and selection of CPI targets can provide an opportunity for the
136 synergistic use of CPIs with BATs therapies for HR+/HER2- patients.

137 Computational modeling integrates diverse measurements to provide insights into
138 how cellular changes affect therapeutic outcomes. Network modeling has revealed
139 therapeutically targetable gene expression mechanisms governing T cell fate selection,
140 function, and exhaustion(20–23), but lacks temporal resolution and cannot account for
141 repeated T cell stimulation in targeted cell therapies. Existing mechanistic models of
142 adoptive T cell therapies have described the emergence of T cell functional states(21–
143 23), but do not address therapeutic dysfunction.

144 To address this gap in knowledge, we developed a dynamic ordinary differential
145 equation (ODE) model that incorporates BATs inhibitory receptor expression profiles. This
146 model predicts the cytotoxic function of each BATs subset and can serve as an *in-silico*
147 testbed to optimize the synergistic use of CPI therapies by targeting the most functional
148 receptors at their peak expression time.

149 Using single-cell transcriptomics and temporal protein and gene expression data,
150 we characterized T cell phenotype emergence and receptor expression dynamics. These
151 data, combined with tumor cytotoxicity profiles, were analyzed using a multivariate
152 statistical framework to predict the relative contributions of BATs subspecies to tumor
153 cytotoxicity.

154 Our ODE model of BATs-mediated tumor killing was constructed from matched
155 temporal protein expression and cytotoxicity data to validate our multivariate analysis
156 findings. Both our multivariate statistical analysis and kinetic-dynamic model identified the
157 LAG3+ BATs subset as a key driver of tumor reduction across multiple donors and cancer
158 cell lines. These results suggest targeting LAG3 in BATs-CPI combinatorial therapies
159 could significantly improve therapeutic outcomes in HR+/HER2- breast cancer patients.

160

161 **MATERIALS AND METHODS**

162 **Target cell coculture**

163 MCF-7, CAMA1, and T47D cells were acquired from ATCC. Cells were thawed in the
164 media suggested by the manufacturer. MCF-7 cells were passaged in cRPMI (RPMI1640
165 + 10%FBS). CAMA1 and T47D cells were gradually acclimated to cRPMI by subsequent

166 passages in mixed (RPMI/native) media with gradually increasing RPMI proportions.
167 Cells were passaged every 2-3 days to avoid confluence.
168
169 **ATC generation**
170 Activated T cells (ATC) were generated using T cells collected from donor PBMC. Blood
171 was collected from normal donors and PBMC were obtained by Ficoll-Paque density
172 gradient separation, counted, suspended in RPMI supplemented with 100 U/mL IL-2 and
173 20 ng/mL OKT3 to activate T cells and stimulate proliferation(24). T cells were expanded
174 by refreshing the cultures with RPMI containing 100 U of IL-2/mL every 2-3 days for 14
175 days. The expanded T cells were harvested and cryopreserved at $100e^6$ viable cells
176 (vc)/mL at -160°C in LN2 until use. ATC used in this study were collected from three
177 donors. Donor information was anonymized prior to the experiment with the exception of
178 sex. Two donors were female and one donor was male.
179
180 **HER2-targeting Bispecific Antibody Preparation**
181 The HER2-targeting bispecific antibody (HER2bi) was generated by chemical
182 heteroconjugation of OKT3, a murine IgG2a anti-CD3 monoclonal antibody (Miltenyi
183 Biotec), and Herceptin, a humanized anti-HER2 IgG1 monoclonal antibody, using sulfo-
184 succimidyl 4-(N-Maleimidomethyl) cyclohexane-1-carboxylate (Sulfo-SMCC) and Traut's
185 reagents as described previously(25). An SDS-PAGE analysis of the HER2bi used in this
186 study is shown in **Fig S1**.
187
188 **BATs preparation**

189 BATs were prepared as described(26). Briefly, ATC were thawed at 37°C, resuspended
190 in RPMI, and washed 2x in RPMI. Washed ATC were resuspended in RPMI + 50 ng/10^6
191 vc anti-HER2x anti-CD3 bispecific antibody (HER2Bi) and rocked on a rocking platform
192 for 15 minutes to allow for HER2Bi to attach to ATC to generate HER2 BATs(27). HER2
193 BATs were washed 3x to remove excess biab and resuspended at 10^6 vc/mL. A pictorial
194 description of BAT generation can be found in **Fig S2**.
195

196 **Single-cell cellular indexing of transcriptomes and epitopes by sequencing (CITE-**
197 **seq) Analysis**

198 ATC from 3 donors were thawed and split into two groups per donor. One group from
199 each donor was armed as described above to generate BATs. Each group was cocultured
200 for 1 hours with MCF7 tumor cells at a 10:1 BAT:MCF7 ratio. BATs were then collected
201 and measured using 10X Genomics CITE-seq technology(27). TotalSeq^{TM}-B
202 oligonucleotide-labeled antibodies for CD45RA, CD3, CD4, CD8, CD69, and CD25 were
203 included in the CITE-seq panel, and cells were stained following the manufacturer's
204 protocol (BioLegend). CITE-seq libraries were processed in parallel following 10X
205 Genomics Single Cell 3' protocol and sequenced on an Illumina NextSeq 500.
206 Raw protein tag and transcriptomic data from each donor were integrated into a Seurat
207 object using the Seurat 5.0 R package(28). Each object was filtered to remove cells with
208 < 500 features or > 2500 features, as well as those with < 1% or > 5% mitochondrial DNA.
209 Data within each object was normalized and the 3000 most variable features were
210 identified. All 6 objects were integrated into a single object using Seurat
211 FindIntegrationAnchors and IntegrateData functions. Data was then scaled, and a

212 principal component analysis (PCA) was conducted to identify the top 100 principal
213 components (PCs). A K nearest-neighbor graph was constructed using the top 25 PCs
214 and used to identify cell clusters. A uniform manifold approximation and projection
215 (UMAP) plot for visualization was created using these clusters. Differential gene
216 expression was used to identify T cell clusters. Briefly, a Wilcoxon Ranked Sum test was
217 run using Seurat's FindAllMarkers function. Genes strongly differentiating each cluster
218 were cross-referenced with T cell literature to identify the phenotype in question.
219

220 **Real-time cell analysis (RTCA) measurements**

221 The xCelligence RTCA monitor was used to measure tumor cell death across the course
222 of the assay. xCelligence plates were zeroed with RPMI prior to seeding(29). In brief, 2e4
223 vc target breast cancer cell lines cultured in RPMI1640 supplemented with 10% FBS were
224 added to each xCelligence well and allowed to adhere. Incubator conditions were
225 maintained at 37 °C and 5% CO2. After 24 hours, BATs were added to each well at
226 predefined ratios between 0.125 – 2 BATs:Tumor. As a surrogate for cytotoxicity,
227 conductivity measurements were recorded continuously for 120h.
228

229 **BATs coculture preparation**

230 Time-course samples were prepared by coculturing BATs and tumor cells at an effector:
231 target ratio of 1:1. Flat bottom 24 well plates were seeded with MCF-7 cells in RPMI at
232 1.2e5 vc/mL and incubated for 24 hours. After 24h, BATs were added at a E:T as
233 determined by target cell counts from a sample plate. Bat-tumor cocultures were

234 incubated for up to 72 hours. Samples were collected from wells at 4, 24, 48, and 72
235 hours. Collected samples were used for flow cytometry readings.
236
237 **Checkpoint inhibitor testing**
238 To test the effects of checkpoint inhibitors on BAT function, RTCA plates were seeded
239 with 2x 10^4 vc/well MCF7 cells, allowed to adhere, and grown for 24 hours. Conditions
240 and media were identical to those described above. BATs were then mixed with either
241 10.0, 3.2, 1.0, 0.32, 0.1, 0.032, or 0 ug/mL Tiragolumab biosimilar InVivoSIM anti-human
242 TIGIT or Relatlimab biosimilar InVivoSIM anti-human LAG3, incubated for 30 minutes at
243 37C, then transferred at a 1:1 BAT:Tumor ratio into corresponding RTCA wells. BAT-
244 tumor cocultures were incubated for up to 72 hours. An identical setup in 96 well plates
245 was performed separately to generate flow cytometry samples. Samples were collected
246 from wells at 4, 24, 48, and 72 hours. Collected samples were used for flow cytometry
247 readings.
248
249 **Flow Cytometry**
250 Flow cytometry stain panels (**Table 1**) were created by mixing fluorescence-conjugated
251 antibody stains targeting the ligands of interest. The following panels were generated:
252 Inhibitory (CD45, CD4, CD8, TIGIT, PD-1, LAG3, TIM-3, CTLA, BTLA), Stimulatory
253 (CD45, CD4, CD8, 4-1BB, CD27, OX40, GITR, HVEM, LIGHT, ICOS), and Coexpression
254 (CD45, CD4, CD8, 4-1BB, 4-1BBL, OX40, TIGIT, PD-1, LAG3). Cells were resuspended,
255 counted for viability, stained in 4 °C DPBS, and fixed before fluorescent intensity readings
256 were acquired on the NovoCyte 3005 3 laser cytometer. Collected data was compensated

257 and analyzed using FlowJo flow cytometry data analysis software. Cells were identified
258 using size and complexity characteristics identified from a T cell-only control sample. Live
259 cells were identified using LIVE/DEAD Fixable Violet Dead Cell stain kit. T cells were
260 further separated from tumor cells by either CD3 or CD45 expression. T cells were further
261 subset using anti-CD4 and anti-CD8 antibodies. A sample flow gating strategy is shown
262 in **Fig S3**. The MFIs of each target stain can be seen in **Fig S4**. Prevalence of each
263 receptor was calculated by percentage expression within CD4 or CD8 subsets.

Panel	Marker/ Analyte	Reagent/ Analyte Detector	Fluorochrome / Reporter	Source / Vendor	Clone	Dilution/ conc.	RRID
Inhibitory Panel	**CD3**	Anti-CD3	APC	BD	HIT3a	1:5	AB_398592
	CD4	Anti-CD4	AF700	Biolegend	A161A1	1:25	AB_2616933
	CD8	Anti-CD8	APCCY7	BD	RPA-T8	1:25	AB_396865
	CTLA4	Anti-CTLA4	PECY5	BD	BNI3	1:25	AB_396177
	BTLA	Anti-BTLA	PECY7	Biolegend	MIH26	1:25	AB_2629566
	PD-1	Anti-PD-1	BV650	BD	EH12.1	1:25	AB_2738595
	TIGIT	Anti-TIGIT	PE	Biolegend	A15153G	1:25	AB_2632729
	LAG3	Anti-LAG3	BV785	Biolegend	11C3C65	1:25	AB_2716126
	TIM-3	Anti-TIM-3	PerCPEF710	Invitrogen	F38-2E2	1:25	AB_11041821
Coexpression Panel	**CD45**	Anti-CD45	PECY5	Biolegend	HI30	1:25	AB_314397
	CD4	Anti-CD4	AF700	Biolegend	A161A1	1:25	AB_2616933
	CD8	Anti-CD8	APCCY7	BD	RPA-T8	1:25	AB_396865
	OX40	Anti-OX40	FITC	Biolegend	Ber-ACT35	1:25	AB_10661725
	4-1BBL	Anti-41BBL	PECY7	Invitrogen	4H3	1:25	AB_2688229
	PD-1	Anti-PD-1	BV650	BD	EH12.1	1:25	AB_2738595
	TIGIT	Anti-TIGIT	PE	Biolegend	A15153G	1:25	AB_2632729
	LAG3	Anti-LAG3	BV785	Biolegend	11C3C65	1:25	AB_2716126
	4-1BB	Anti-4-1BB	APC	Biolegend	4B4-1	1:25	AB_830671
Stimulatory Panel	**CD45**	Anti-CD45	BV786	Biolegend	HI30	1:25	AB_314397
	CD4	Anti-CD4	AF700	Biolegend	A1616A1	1:25	AB_2616933
	CD8	Anti-CD8	APCCY7	BD	RPA-T8	1:25	AB_396865
	OX40	Anti-OX40	FITC	Biolegend	Ber-ACT35	1:25	AB_10661725
	LIGHT	Anti-LIGHT	PECY7	Biolegend	T5-39	1:25	AB_2721659
	ICOS	Anti-ICOS	PerCPEF710	Invitrogen	ISA-3	1:25	AB_10854730
	HVEM	Anti-HVEM	APC	Biolegend	122	1:25	AB_2565252
	CD27	Anti-CD27	BV510	BD	L128	1:25	AB_2737998
	4-1BB	Anti-41BB	PE	BD	4B4-1	1:5	AB_396252
	GITR	Anti-GITR	PECY5	Biolegend	621	1:25	AB_2240646

264
265 **Table 1:** Targets for fluorescent antibodies included in each flow cytometry panel.
266

267 **OPLS-R analysis**

268 An orthogonalized partial least squares (OPLS)-regression model was built to predict the
269 impact of BATs receptor expression on tumor reduction. BATs were binned into distinct
270 groups by their expression of CD8 and CD4, and again by their expression of PD-1, TIGIT,
271 and/or LAG3. Triplicate counts were averaged within donor and against target cell line.
272 These counts were inputted to predict the changes in tumor cell count and the rate of
273 change in tumor counts as measured by RTCA. Separate models were created for the 3-
274 donor study and the 3-target study.
275 Inputs for tumor counts or rate of change compared against BATs counts were taken at
276 a set time interval from the time of BATs collection. Models for each study were created
277 with 0, 1, 4, 12, and 24-hour intervals from the time of BATs collection to increase the
278 robustness of model predictions. The variable importance in projection (VIP) scores for
279 each BATs subset were calculated(30), ranked, and artificially oriented in the direction of
280 their loadings on latent variable 1 (LV1). The directionality of groups with VIP scores >1
281 was used to predict the positive or negative impact on tumor growth for each
282 receptor/ligand.
283

284 **ODE model construction and testing**

285 An ODE model was constructed using mass action equations to describe changes in
286 tumor cell count. The following equation was used to describe tumor cell count.

287 $$\frac{dTumor}{dt} = a_{TP} * Tumor - \frac{a_{TP} * Tumor^2}{Max_{Tumor}} - \left(a_{Kill_N} * NBATs * Tumor\right)$$

288 $$- \left(a_{Kill_L} * LBATs * Tumor\right) - \left(a_{Kill_P} * TBATs * Tumor\right)$$

289 $$- \left(a_{KillD} * DBATs * Tumor\right)$$

290 The first two terms represent tumor growth in the absence of BATs, and the next four
291 negative terms represent the contribution of each BAT subset to the rate of tumor cell
292 clearance. Tumor growth rate was assumed to be sigmoidal, and was fit to data collected
293 from the control 0:1 BATs:Tumor condition during the RTCA experiment. NBATs (LAG3-
294 TIGIT- CD8s), TBATs (LAG3- TIGIT+ CD8s), LBATs (LAG3+ TIGIT- CD8s), and DBATs
295 (LAG3+ TIGIT+ CD8s) rate of change were determined by taking the derivative of spline
296 functions fit to the flow cytometry cell counts collected at 0, 4, 24, 48, and 72 hours.
297 The CaliPro parameter optimization package was used to determine the potential ranges
298 and optimal values for each species rate parameter (31). CaliPro optimizes unknown
299 model parameters by creating a parameter space using Latin Hypercube Sampling within
300 parameter-specific ranges set by the user. Each parameter was tested by software, and
301 parameter sets that meet a user-defined set of criteria are used to generate a new LHS
302 parameter space for a second iteration. This procedure continued until a large enough
303 portion of parameters met the acceptance criteria. The final parameter space contains a
304 refined range of parameters which best describe the system in question. Acceptable
305 parameter spaces were those that generated tumor counts within +/- 10% of the
306 measured values at 0, 4, 12, 24 ,36, 48, 60, and 72 hours.
307
308
309 **RESULTS**
310 **Bispecific antibody-driven interactions generate highly cytotoxic LAG3+ effector T**
311 **cell populations after 1 hour exposure to target cells**

312 HER2 BATs were generated by arming activated T cells from donor PBMC with a HER2-
313 targeting bispecific antibody (**Fig S1**) (Materials and Methods) and cocultured with HR+
314 breast cancer cells. To identify phenotypic changes in T cells driven by the engagement
315 of T cell receptor (TCR) and tumor antigen mediated by the BiAb, we profiled
316 transcriptional and protein expression changes in HER2 BATs and unarmed ATC after
317 exposure to tumor cells using CITE-seq (**Fig 1A**). The matched protein and RNA data
318 were integrated and pooled, and an unsupervised graph-based clustering method was
319 applied to generate 12 cell clusters (**Fig 1B**). CD4 and CD8 protein tags were used to
320 identify major T cell populations, while CD69 and CD45RA protein tags helped
321 differentiate between resting, dividing, and activated T cell subsets (**Fig 1B, Fig S5**).
322 These 12 cell subsets exhibited varying transcriptomic expression profiles of cytotoxic
323 factors, inhibitory receptors, costimulatory receptors, and relevant transcription factors
324 (**Fig 1D**). Wilcoxon ranked-sum testing was used to identify marker genes distinguishing
325 each group (**Fig 1C**) to assist in applying known T cell phenotypes.
326 The presence of the BiAb drove phenotypic changes in both CD4 and CD8 T cells (**Fig**
327 **1A, B**). Activated CD4 BATs, indicated by CD69 protein expression, switched primarily to
328 a pro-inflammatory T helper 1 (Th1) phenotype (**Fig 1C**, **Fig S5**). A smaller subset of
329 activated CD4 BATs was observed to adopt a humoral Th2 phenotype (**Fig 1B**), which
330 not only drives B cells to produce immunoglobulins but may also facilitate tumor
331 progression(32). The Th1 population was comprised primarily of BATs, which accounted
332 for 82% of the population, while the Th2 population was evenly split between BATs (46%)
333 and ATC (54%). CD8 BATs displayed progressive activation: a mid-activation group,
334 labeled CD8_Act, was CD45RA-CD69+, while a fully activated effector group, labeled

335 CD8_Eff, was CD45RA+CD69+. Additionally, two smaller BATs groups, an NK-like (NKT)
336 group marked by KLRD1(33) and FCER1G(34) and mucosal-associated invariant (MAIT)
337 group marked by KLRB1(35) and NCR3(36), were also present. The CD8_Eff group was
338 identified as the primary cytotoxic group, as demonstrated by high expression of
339 granzyme (GZMA, GZMB, GZMK, GZMH) and perforin (PRF) genes, as well as
340 inflammatory cytokine (IFN-γ, TNF-α) and FAS ligand expression (**Fig 1D**). The CD8_Eff
341 group was also enriched in EOMES and TBX21, two transcriptional regulators associated
342 with T cell maturation, terminal differentiation, and effector function(37), further indicating
343 the role of this group as an effector T cell (**Fig 1D**). TCF7, a transcriptional regulator
344 indicating a pre-antigen encounter T cell state(38), was downregulated in the CD8_Eff
345 group, while TOX, a gene associated with T cell effector function and exhaustion(39), was
346 upregulated (**Fig 1D**).
347 Strong cytotoxic potential was observed to correlate with targetable inhibitory and
348 costimulatory receptor expression (**Fig 1D**). The cosignaling receptors LAG3 and TIGIT,
349 which directly modulate BATs cytotoxicity, were enriched in the CD8_Eff group (**Fig 1E**).
350 While expression of PD-1 (PDCD1), TIM3 (HAVCR2), and CTLA4 was detected in the
351 CD8_Eff group (**Fig 1D**), their levels were low and not significantly different from those in
352 the total cell population.
353 Costimulatory receptors 4-1BB (TNFRSF9), ICOS, CD27, HVEM (TNFRSF14), and
354 LIGHT (TNFSF14) were observed in the CD8_Eff group (**Fig 1D**). LIGHT and ICOS
355 expression were upregulated in all activated BATs groups but were not significantly
356 upregulated in the CD8_Eff group (**Fig 1D**). CD27 was present but downregulated
357 compared to other CD8 groups (**Fig 1D**), indicating terminal effector differentiation(40).

358 Only 4-1BB expression was significantly upregulated in the CD8_Eff group (See
359 **Discussion**).
360 While LAG3 expression was observed throughout the CD8_Eff group, TIGIT expression
361 was concentrated within a subset of these cells (**Fig 1E, F**). Comparison between
362 $TIGIT_{High}$ and $TIGIT_{Low}$ CD8_Eff cells reveals distinct expression of regulatory genes
363 associated with T cell effector differentiation. $TIGIT_{High}$ CD8_Effs are enriched for EOMES
364 and CMC1, while $TIGIT_{Low}$ CD8_Effs are enriched for HOPX and SPRY1. All four genes
365 are involved in T cell effector differentiation(37, 41–43), but the absence of overlap may
366 indicate a potential divergence in function between $TIGIT_{High}$ and $TIGIT_{Low}$ CD8_Eff cells.
367 These expression patterns may indicate that highly cytotoxic CD8 BATs are more strongly
368 regulated by TIGIT or LAG3 after initial interaction with breast cancer tumor cells and
369 might benefit from CPI therapies targeting these receptors. Likewise, 4-1BB agonism may
370 provide costimulatory signals preferentially to a highly cytotoxic subpopulation.
371
372 **Temporal profiling reveals distinct dynamics of costimulatory and inhibitory**
373 **receptor expression following tumor exposure**
374 The emergence of therapeutically targetable cosignaling receptors as marker genes for
375 highly cytotoxic effector cells after 1 hour of exposure suggests promising potential for
376 effective combinatorial BATs therapies. To determine whether the observed expression
377 patterns of TIGIT, LAG3 and 4-1BB from CITE-seq data persist beyond 1 hour of
378 stimulation and whether transcriptomic expression patterns translate to expression of
379 surface proteins we analyzed surface receptor expression on BATs cocultured with the
380 breast cancer cell lines. The coexpression dynamics of inhibitory and stimulatory

381 receptors on BATs were profiled over a 72-hour coculture with HR+ tumor cells (**Fig 2A**).
382 Flow cytometry panels used to profile receptor expression were designed based on gene
383 expression values observed in **Fig 1D** and are detailed in **Table 1**.
384
385 *CD4 BATs preferentially express PD-1, which coexpresses with LAG3 and TIGIT*
386 CD4 BATs expressed PD-1, TIGIT, and LAG3 during the initial 72-hour challenge (**Fig**
387 **2B**). CD4 BATs preferentially expressed PD-1, while LAG3 and TIGIT were primarily
388 coexpressed on PD-1 expressing cells (**Fig 2E**). ICOS expression within the CD4 pool
389 gradually increased with time, while CD27 expression dipped over 24h before rebounding
390 (**Fig S6A**). Th1 CD4 cells expressed PD-1 significantly higher than other BATs groups in
391 our CITE-seq data, potentially suggesting the immediate emergence of a Th1 CD4 subset
392 (**Fig 1D**). Th1 CD4 cells expressed PD-1 significantly higher than other BATs groups in
393 our CD4 data, potentially suggesting the immediate emergence of a Th1 CD4 subset.
394
395 *CD8 BATs rapidly express LAG3 and 4-1BB while gradually increasing PD-1 and TIGIT*
396 *expression*
397 The inhibitory panel showed that CD8 BATs preferentially expressed LAG3 (**Fig 2 B, C**).
398 TIGIT and PD-1 were observed to a lesser extent on CD8 T cells, and primarily
399 coexpressed with LAG3 (**Fig 2 C, E, Fig S7**). TIM3, CTLA4, and BTLA were minimally
400 expressed by BATs over the 72 hours duration of the experiment. In all samples, LAG3+
401 CD8 BATs hit a proportional and numerical high between 24 and 48 hours after coculture,
402 before declining across the remaining assay duration. PD-1 and TIGIT expression
403 gradually increased as the assay progressed. Interestingly, samples that maintained a

404 higher proportion of LAG3+ CD8 T cells throughout the assay cleared a greater proportion
405 of tumor cells cumulatively across 72 hours. A stimulatory receptor profile demonstrated
406 CD8 BATs primarily expressed 4-1BB and ICOS, with 4-1BB spiking rapidly during the
407 first 24h before exiting the system and ICOS gradually increasing with time. CD27, which
408 was strongly expressed at t = 0 hours, rapidly decreased in expression during the first 24
409 hours, before recovering to initial expression levels during the last 48 hours of the
410 experiment (**Fig S6A**). Costimulatory receptor expression overlap was minimal, with the
411 exception of CD27 coexpression (**Fig S6B**). The presence of LAG3, TIGIT, and 4-1BB
412 indicates the CD8 BATs are primarily the CD8_Eff phenotype observed in our CITE-seq
413 data.
414 A coexpression panel was designed to explore overlap between costimulatory and
415 inhibitory receptors (**Fig 2D, F**). Expression of coinhibitory receptors reflected what was
416 observed on the inhibitory panel – LAG3 and PD1 expression dominated CD8 and CD4
417 BATs, respectively, with both PD-1 and TIGIT coexpressing with LAG3 at increasing
418 frequency on CD8s (**Fig 2D, F**). PD-1 and TIGIT rarely coexpressed on CD8s in the
419 absence of LAG3. Interestingly, 4-1BB strongly coexpressed with LAG3 on CD8s during
420 the first 24h (**Fig 2D, F**). LAG3 and 4-1BB presence simultaneously peaked at 24 hours,
421 and LAG3 and TIGIT remained the primary inhibitory receptors after 24 hours, (**Fig 2D,**
422 **F**), which suggests that 4-1BB expression or stimulation precedes T cell activation
423 pathways that preferentially express LAG3 and/or TIGIT.
424
425 **Multivariate statistical analysis predicts opposing effects of LAG3 and TIGIT**
426 **expression on BATs-mediated tumor cell cytotoxicity rates**

427 We hypothesized that LAG3, TIGIT, and PD-1 represent distinct anti-tumor functional
428 phenotypes, with their expression kinetics closely correlating with changes in BATs
429 function and phenotype. PD-1 was enriched in activated Th1 and Th2 CD4 subgroups but
430 did not associate strongly with CD8_Eff in our CITE-seq data (**Fig 1D**). LAG3 and TIGIT
431 correlated strongly with components of cytotoxic pathways in our CITE-seq data (**Fig 1D**)
432 and suggests a highly cytotoxic activated effector state in BATs. However, TIGIT was only
433 partially enriched within our CD8_Eff group and correlated with regulatory components
434 associated with effector cell maturation (**Fig 1D**). A Partial Least Squares Regression
435 (PLS-R) model was constructed to determine if tumor cell reduction cytotoxicity could be
436 predicted by receptor presence (**Fig 3A, B**). Cells were binned by CD4/CD8, TIGIT,
437 LAG3, and PD-1 expression, with cells expressing combinations of these receptors put in
438 unique bins. The prevalence of each phenotype at each timepoint was used to predict the
439 rate of tumor cytotoxicity measured by RTCA at 4 hours post-receptor measurement. Our
440 model predicted 98% of the variance seen in the rate of tumor growth and reduction, and
441 outperformed 1000 random permutations of the data ($p < 0.001$) (**Fig 3A**). Examining the
442 top predictors of the cytotoxicity, which were defined as those with VIP >1, we observed
443 that CD8 BATs expressing LAG3 with or without PD-1 correlated with increased rates of
444 cytotoxicity, while TIGIT expression on either CD8 or CD4 cells was negatively correlated
445 with the rate of cytotoxicity (**Fig 3 B, C**). Cells expressing a combination of LAG3 and
446 TIGIT, regardless of PD-1 expression, were not predictive. Cells expressing none of the
447 three receptors were negatively correlated with cytotoxicity, similar to TIGIT expressing
448 cells, potentially suggesting a pre-activated state. In summary, our data show that the
449 expression of LAG3 on BATs is significantly associated with anti-tumor cytotoxicity, while

450 TIGIT expression dampens BATs-driven cytotoxicity (**Fig 3C, Fig S8**). Considering these
451 results, we predict CD8 BATs will fall into one of 4 generalized functional groups: NBATs
452 (LAG3-/TIGIT-), LBATs (LAG3+/TIGIT-), TBATs (LAG3-/TIGIT+), and DBATs
453 (LAG3+/TIGIT+), with exposure to tumor cells driving the transfer of BATs from a LAG3
454 and/or TIGIT negative group to a LAG3 and/or TIGIT positive group (**Fig 3D**).
455

456 **Mechanistic modeling identifies LAG3 BATs as key drivers of tumor reduction**

457 The PLS-R model indicates that the balance of BATs subsets defined by receptor
458 expression plays a crucial role in tumor reduction. To more directly determine the
459 functional impact of each subset and validate our PLS-R findings, an ODE-based dynamic
460 model of tumor-BATs interactions was constructed (See Methods). Surviving tumor cell
461 counts were extracted from RTCA data, while BATs subset counts were extracted from
462 receptor expression measured by the coexpression flow cytometry panels. Given the
463 homogeneity in CD4 population dynamics across experiments, cytotoxic CD8 cells were
464 selected for the development of the model. Cytotoxic potential as predicted for each
465 subset by the PLS-R model was used to define four functional groups in the kinetic-
466 dynamic BATs-tumor model. Specifically, the PLS-R model predicted LAG3 and TIGIT
467 expression have significant but opposing effects on the rate of tumor expansion or
468 survival. LAG3 expression predicts higher rates of tumor reduction, while TIGIT predicts
469 weaker tumor reduction. The expression of PD-1 was not predictive. Based on the above
470 findings, a mechanistic model of tumor-BATs interactions was constructed consisting of
471 tumor cells and 4 receptor-defined BATs species: LAG3-/TIGIT- BATs (NBATs),

472 LAG3+/TIGIT- BATs (LBATs), LAG3-/TIGIT+ BATs (TBATs), and LAG3+/TIGIT+ BATs
473 (DBATs) (**Fig 4A**).
474 Our ODE model was constructed and distinct cytotoxicity rates were estimated for each
475 BATs phenotype, accurately replicating tumor cell count dynamics over a 72-h BAT-tumor
476 coculture. Tumor growth rates were determined by fitting experimental tumor growth data
477 to sigmoidal curves, using maximum cell counts observed in tumor-only control
478 conditions. Experimentally collected BATs counts were modeled using spline functions to
479 represent dynami changes in BATs numbers over time. CaliPro, an iterative parameter
480 optimization package, was employed to estimate the cytotoxicity parameter space. Value
481 ranges for cytotoxicity rates for each BAT phenotype were identified to best match
482 experimental BATs-tumor dynamics (**Fig 4B**). Finally, estimated cytotoxicity rates and the
483 total number of tumor cells killed by each BATs subpopulation were compared as key
484 metrics to evaluate the cytotoxic potential of each cell phenotype.
485 When comparing a single donor across 3 HER2-/HR+ breast cancer cell lines, LBATs
486 emerge as the clear driver of cytotoxicity (**Table 2** and **Fig 4C**). LBATs demonstrate a
487 larger capacity for tumor clearance both through a higher cytotoxicity rate (**Table 2**) and
488 greater number of tumor cells removed compared to all other species (**Fig 4C**). This
489 model prediction matches the functional potential observed in our PLS-R model, where
490 LAG3+ BATs correlated with greater tumor reduction (**Fig 3B**), and our CITE-seq data,
491 where LAG3+ CD8_Eff cells expressed significantly higher granzyme and perforin
492 concentrations than other observed groups (**Fig 1D**). Both factors make the generation
493 of these cells highly desirable therapeutically. Additionally, LAG3+ BATs were observed
494 to proliferate strongly in all systems, indicating they can sustain an effective anti-tumor

495 response when generated. DBATs, which expressed both LAG3 and TIGIT, were observed to also contribute to cytotoxicity, although at a lower rate than LBATs (**Fig 4C**). NBATs were 5.75-fold less cytotoxic than LBATs, although their presence as the most populous BAT subtype meant they contributed significantly to tumor removal. TBATs demonstrated significantly lower cytotoxicity compared to either LAG3+ subgroups LBATs or DBATs and remained at low enough numbers to contribute minimally to tumor reduction.

Parameter	Target		
	MCF7	CAMA1	T47D
Tumor growth rate	0.13	0.06	0.16
Max conductivity	1.4	3.2	1.2
LBAT Cytotoxicity Rate (Range)	1.18E-06 (1.01E-06 - 1.34E-06)		
NBAT Cytotoxicity Rate (Range)	1.95E-07 (1.31E-07 - 1.97E-07)		
DBAT Cytotoxicity Rate (Range)	9.54E-07 (6.61E-07 - 9.63E-07)		
DBAT Cytotoxicity Rate (Range)	9.54E-07 (6.61E-07 - 9.63E-07)		

Table 2: Optimal parameters and ranges determined by CaliPro meeting pass criteria for Donor 1 BATs challenged against 3 tumor cell lines.

Comparisons across donors revealed consistent patterns of cytotoxicity. While the behavior of BATs derived from different donors could not be described using identical parameter sets, individual models predicted LBATs as the most cytotoxic subset, followed by DBATs, with

Parameter	Donor		
	Donor 1	Donor 2	Donor 3
Tumor growth rate	0.0748		
Max conductivity	7.6		
LBAT Cytotoxicity Rate (Range)	1.18E-06 (1.01E-06 - 1.34E-06)	8.59E-06 (8.38E-06- 1.16E-05)	5.28E-06 (3.89E-06 - 5.95E-06)
NBAT Cytotoxicity Rate (Range)	1.95E-07 (1.31E-07 - 1.97E-07)	4.48E-08 (2.17E-08 - 4.91E-08)	4.49E-07 (5.61E-08 - 7.48E-07)
DBAT Cytotoxicity Rate (Range)	9.54E-07 (6.61E-07 - 9.63E-07)	3.71E-06 (7.90E-07 - 4.35E-06)	1.33E-06 (1.27E-06 - 5.52E-06)
TBAT Cytotoxicity Rate (Range)	3.98E-07 (3.23E-07 - 4.25E-07)	8.59E-08 (5.42E-08 - 5.74E-07)	3.36E-07 (3.34E-07 - 7.31E-07)

Table 3: Optimal parameters ranges determined by CaliPro meeting pass criteria for BATs from three donors challenged against MCF7 tumor cells.

518 NBATs and TBATs alternating as the least and second least cytotoxic subgroup (**Fig 5B-**
519 **C, Table 3**).
520
521 Notably, Donor 2, which demonstrated the lowest tumor cell clearance, relied more
522 heavily on its DBATs for tumor reduction. This likely resulted from a higher relative
523 abundance of DBATs generated during the coculture experiment compared to Donors 1
524 and 3.
525
526 Across all donors, LAG3 emerged as a robust indicator of effector cytotoxicity, suggesting
527 that the LAG3+ CD8 BATs subset plays a primary role in tumor elimination during HR+
528 breast cancer-HER2 targeted BATs immunotherapy. While LAG3 has known inhibitory
529 functions, it is known to be upregulated on activated cytotoxic T cells, and its presence
530 on BATs appears to indicate a functional cytotoxic cell. In contrast, TIGIT expression in
531 BATs cells may act either as a suppressor of cytotoxic function or an indicator of further
532 dysfunction. To test whether the activation of either receptor was responsible for the
533 differences in cytotoxicity observed in each species, the 3-donor experiment was
534 repeated in the presence of varying concentrations of either an anti-LAG3 Relatlimab
535 biosimilar or an anti-TIGIT Tiragolumab biosimilar (**Fig S9A**). The addition of anti-LAG3
536 generated a modest increase in cytotoxicity in Donors 1 and 3, which had higher
537 proportions of LAG3+ CD8 BATs (**Fig S9B**). While it is not likely that MCF7 cells express
538 LAG3 ligands MHC-II or FGL-1, LAG3 is known to be autoinhibitory, and thus the addition
539 of LAG3 may prevent this autoinhibitory action in BATs. The addition of anti-TIGIT did not
540 have a positive effect on BAT cytotoxicity for any donor, suggesting that TIGIT is not

541 activated in this system (**Fig S9C**). As MCF7 cells are not known to express TIGIT ligands
542 PVR, NECTIN1, or NECTIN2, the lack of efficacy is not surprising and suggests that TIGIT
543 presence in our system indicates less functional BATs. Future in vivo studies should test
544 the impact of these checkpoint blockades on BATs when in the presence of LAG3 or
545 TIGIT ligands to confirm these results.
546

547 **DISCUSSION**

548 Changes in receptor expression as a function of differentiation likely reflect the T cell's
549 capacity to mount diverse and multifunctional immune responses against perceived
550 threats. Understanding how these phenotypes emerge, and function can significantly
551 enhance our ability to engineer T cells for predictable and effective responses against
552 tumors or pathogens. In this study, we characterized emerging T cell subtypes in BATs
553 challenged by HR+ HER2- breast cancers and developed a model combining T cell
554 inhibitory receptor expression dynamics with cytotoxicity rates to identify associations
555 between targetable pathways of T cell inhibition and T cell anti-tumor cytotoxicity.
556 While inhibitory receptor expression is intrinsically linked with T cell stimulation, the
557 factors driving differential expression remain unclear(44–46). Across three donors and
558 when challenged with 3 HR+ breast cancer cell lines, only TIGIT, LAG3, and PD-1 were
559 expressed within the first 72 hours of challenge. This suggests that combinatorial
560 therapies pairing BATs with CPI therapies should prioritize these receptors.
561 Our model indicates an association between TIGIT surface expression and reduced BATs
562 function. Because TIGIT ligands PVR, NECTIN1, and NECTIN2 have been detected in
563 breast cancer and correlate with poor prognostic outcomes, the loss of function in TIGIT+

564 cells may result of TIGIT-ligand driven inhibition(47, 48). Blocking TIGIT may reverse the
565 suppressive regulatory effect and augment the cytotoxicity of TIGIT+ and LAG3+/TIGIT+
566 subset of BATs. However, TIGIT presence on T cells may indicate a more terminally
567 differentiated and exhausted state. Coexpression of TIGIT with other inhibitory receptors,
568 including PD-1 and LAG3, is a hallmark of T cell dysfunction in tumors(49–52). Because
569 we observe TIGIT expression primarily in tandem with PD-1 or LAG3, these cells may be
570 terminally exhausted and less capable of mediating cytotoxic activity even if TIGIT
571 activation or activity is blocked.
572 LAG3+ cells do not appear to be inhibited in our model. LAG3 expression in the absence
573 of other inhibitory receptors, such as TIGIT or TIM-3, is a hallmark of cytotoxic effector T
574 cell activation(53–55). LAG3 has been observed as primarily regulating effector functions
575 like cytotoxicity for tumor-targeting T cells, and thus LAG3 expression by BATs may
576 indicate a highly functional effector group(56, 57). These studies also observe PD-1 as
577 primarily responsible for inhibiting cell proliferation, and thus the lack of PD-1 on our
578 LAG3+ population may facilitate the proliferation observed in this population. The primary
579 LAG3 ligand, MHC-II, is expressed predominantly on antigen-presenting cells (APCs),
580 and thus should not be present in our coculture system(58). However, as breast cancers
581 can be enriched in APCs, including pro-tumor macrophages, LAG3+ BATs may
582 encounter strong inhibition when applied in vivo(59, 60). Thus, preemptive blockade of
583 LAG3 may ensure these primary cytotoxic cells maintain their function in patients,
584 regardless of APC presence. Additionally, LAG3 has been observed to inhibit T cell
585 cytotoxicity without stimulation(61). Thus, LAG3 blockade may improve BATs function
586 regardless of APC presence.

587 The two-cell, two-dimensional model we generated focuses exclusively on BAT changes
588 that may be triggered through interactions with tumor cells, other T cells, or the cell signals
589 produced by tumors and T cells. In vivo, the TME will contain a far more diverse array of
590 cells and signals, many of which may affect BAT development and expression of LAG3,
591 TIGIT, or related receptors. Other receptors may become more significant players in BAT
592 function and inhibition when BATs are exposed to the wider range of signals in the TME.
593 However, the direct tumor-BAT and BAT-BAT interactions our model accounts for will
594 play a large role in BAT development, and thus the findings here will likely still improve
595 BAT function.
596 Our investigation was limited to the dynamic changes in T cell behavior, without capturing
597 tumor cell ligand expression dynamics. We assumed that components governing the rate
598 of interaction between BATs and target cells remain constant, except for changing
599 cytotoxicity observed in different BATs phenotypes. Furthermore, our coculture system
600 was focused strictly on BiAb-mediated CD8 T cell-tumor interactions and studying signals
601 and secreted factors from other cells was beyond the scope of our work. These factors
602 can influence tumor and T cell behaviors affecting cytotoxicity. TCR-activated CD4 and
603 CD8 T cells are known to produce cytokines and other signaling molecules, including
604 interferon gamma (IFNγ) and tumor necrosis factor (TNFα)(62–64), which affect both T
605 cell function and tumor proliferation(65), and were highly expressed in our CD8_Eff group.
606 While the effect of these cytokines may be captured by the cytotoxicity rates predicted in
607 our model, any compounding effects of their persistent presence or increasing
608 concentration may have not been captured by our model. Because the goal of this project
609 was to characterize CD8 BAT development, CD4 BATs were not included in our

610 mechanistic model. While certainly relevant to tumor clearance, CD4 cells are largely
611 known to be cytokine producing cells, which did not fit in our BAT-Tumor interaction
612 model. CD4 receptor expression was largely similar across donors as well, and thus we
613 assume that their impact is similar across experiments. Limiting the model to CD8 T cells
614 might explain the donor-to-donor variability observed in subset-specific tumor clearance
615 rates (**Table 3**). The initial BAT population for Donor 2 had a much higher proportion of
616 CD4 T cells compared to Donors 1 and 3 and cleared fewer target cells (**Fig S10**). Donor
617 2 began with and generated fewer LAG3+ CD8s, and an increased CD4 proportion
618 demands fewer CD8 cells, so this observation may simply be the result of fewer cytotoxic
619 BATs present. However, CD8 BATs expansion was also lower with higher CD4, and
620 particularly PD-1+ CD4, presence, possibly indicating an inhibitory effect elicited from
621 CD4 BATs. The inclusion of other effector cells might further improve the model fits (**Fig**
622 **5A**) but is outside the scope of this paper.
623 Target cell phenotypic changes also likely change BATs-target interactions but are not
624 captured in our system. Cytokine presence and cell damage can change receptor
625 expression on target cells in a manner that may alter BATs-target interactions with time.
626 Inflammatory cytokines, and in particular Type I interferons, can upregulate inhibitory
627 receptor expression on T cells(66). Similarly, IFNγ can upregulate cognate ligands for
628 inhibitory receptors, such as PD-L1, on tumor cells(67). Cell damage and tumor
629 mutational status can also upregulate these ligands(68–70). Expression of PVR, a TIGIT
630 ligand, has been observed in response to DNA damage, and may be present on some or
631 all the target cells in our system(71). Thus, the target cells in our system may evolve to
632 inhibit BATs expressing certain inhibitory receptors.

633 Preferential generation of more cytotoxic BATs subspecies may improve tumor clearance
634 against HR+ breast cancers. Costimulatory signaling is a crucial part of T cell activation
635 and plays a role in inhibitory receptor expression intensity(72, 73). Both our CITE-seq and
636 flow cytometry data indicate 4-1BB expression is associated with cytotoxic effector BATs.
637 4-1BB was observed to be strongly correlated with LAG3+/TIGIT+ CD8_Eff cells in our
638 CITE-seq data (**Fig 1D**), and 4-1BB ligand expression was strongly correlated with LAG3
639 and TIGIT expression for the initial 24-48h of our coculture experiment before
640 disappearing from our system (**Fig 2D, Fig S6A**). This may indicate that 4-1BB exists to
641 stimulate highly cytotoxic BATs upon their initial encounter with target cells. However, it
642 is unclear if 4-1BB stimulation is associated with TIGIT expression alone, or if it is also
643 linked to LAG3 expression. Further exploration of the impact of 4-1BB stimulation on
644 BATs function and inhibitory receptor expression may provide insight into what incoming
645 signals govern BATs function. If 4-1BB activation changes BATs function, whether to
646 increase or decrease cytotoxicity, utilization of 4-1BB targeting therapies may enhance
647 tumor reduction. A small number of 4-1BBL+ BATs were observed in our system at 4
648 hours, which may be indicative of a self-stimulating T cell subtype previously observed to
649 increase tumor kill in mouse breast cancer models(74). However, the transient nature of
650 both 4-1BB and 4-1BBL makes their utilization as targets difficult.
651 Together, these findings provide a compelling support for the use of predictive statistical
652 analysis and mathematical modeling in the rational design of combination
653 immunotherapies. They also strongly suggest that the anti-solid tumor activity of BATs in
654 our phase I/II metastatic breast cancer clinical trials may be in part driven by the
655 dominance of a LAG3+ cytotoxic phenotype over TIGIT downregulatory activity(12, 13).

656 Our recent phase II trial in hormone refractory prostate cancer (HRPC) that combines the
657 CPI pembrolizumab with HER2 targeted BATs showed significant clinical improvement in
658 clinical responses and improved survival(75) when the use of CPI alone has not been
659 successful in clinical test for HRPC. Furthermore, our recent ongoing trial combining
660 pembrolizumab with HER2 BATs in selected metastatic breast cancer patients heavily
661 pretreated with chemotherapy led to stable disease and improved survival (unpublished).
662 The improvement in patient response to BATs combined with a PD-1/PD-L1 targeting
663 therapy bodes well for further work in this area: our model predicted PD-1 to have a lower
664 impact on BATs function than LAG3 or TIGIT and thus combining BATs with a LAG3 or
665 TIGIT blockade may improve responses to an even greater extent. Further investigations
666 into CPI and BATs combination strategies targeting stimulatory or inhibitory receptors to
667 enhance BATs effector functions will likely improve the potential of BATs therapy in
668 metastatic breast cancers and other solid tumors.

669 **REFERENCES**

670 1. Giaquinto, A. N., H. Sung, K. D. Miller, J. L. Kramer, L. A.
671 Newman, A. Minihan, A. Jemal, and R. L. Siegel. 2022. Breast
672 Cancer Statistics, 2022. *CA Cancer J Clin* 72: 524–541.
673 2. Albarrán, V., M. San Román, J. Pozas, J. Chamorro, D. I. Rosero,
674 P. Guerrero, J. C. Calvo, C. González, C. García de Quevedo, P. Pérez
675 de Aguado, J. Moreno, A. Cortés, and A. Soria. 2024. Adoptive T cell
676 therapy for solid tumors: current landscape and future challenges.
677 *Front Immunol* 15: 1352805.
678 3. Helmich, B. K., and R. W. Dutton. 2001. The role of adoptively
679 transferred CD8 T cells and host cells in the control of the growth of
680 the EG7 thymoma: factors that determine the relative effectiveness
681 and homing properties of Tc1 and Tc2 effectors. *J Immunol* 166:
682 6500–6508.
683 4. Lee, H. J., Y.-A. Kim, C. K. Sim, S.-H. Heo, I. H. Song, H. S. Park,
684 S. Y. Park, W. Seon Bang, I. A. Park, M. Lee, J. H. Lee, Y. S. Cho, S.
685 Chang, J. Jung, J. Kim, S. B. Lee, S. Y. Kim, M. S. Lee, and G. Gong.
686 2017. Expansion of tumor-infiltrating lymphocytes and their potential
687 for application as adoptive cell transfer therapy in human breast
688 cancer. 8: 113345–113359.
689 5. Lum, L. G., A. Thakur, M. Choi, A. Deol, V. Kondadasula, D.
690 Schalk, K. Fields, M. Dufrense, P. Philip, G. Dyson, H. D. Aon, and
691 A. F. Shields. 2020. Clinical and immune responses to anti-CD3 x
692 anti-EGFR bispecific antibody armed activated T cells (EGFR BATs)
693 in pancreatic cancer patients. *Oncoimmunology* 9.
694 6. Grabert, R. C., L. P. Cousens, J. A. Smith, S. Olson, J. Gall, W. B.
695 Young, P. A. Davol, and L. G. Lum. 2006. Human T Cells Armed
696 with Her2/neu Bispecific Antibodies Divide, Are Cytotoxic, and
697 Secrete Cytokines with Repeated Stimulation Cancer Therapy:
698 Preclinical. *Clin Cancer Res* 12.
699 7. Lum, L. G., A. Thakur, Q. Liu, A. Deol, Z. Al-Kadhimi, L. Ayash,
700 M. H. Abidi, C. Pray, E. N. Tomaszewski, P. A. Steele, D. L. Schalk,
701 H. Yano, A. Mitchell, M. Dufresne, J. P. Uberti, and V.
702 Ratanatharathorn. 2013. CD20-targeted T cells after stem cell
703 transplantation for high risk and refractory non-Hodgkin's lymphoma.
704 *Biol Blood Marrow Transplant* 19: 925–933.
705 8. Thakur, A., R. Rathore, S. V. Kondadasula, J. P. Uberti, V.
706 Ratanatharathorn, and L. G. Lum. 2018. Immune T cells can transfer
707 and boost anti-breast cancer immunity. *Oncoimmunology* 7.
708 9. Lum, L. G., A. Thakur, Z. Al-Kadhimi, G. A. Colvin, F. J.
709 Cummings, R. D. Legare, D. S. Dizon, N. Kouttab, A. Maizel, W.
710 Colaiace, Q. Liu, and R. Rathore. 2015. Targeted T-cell therapy in
711 stage IV breast cancer: A phase i clinical trial. *Clinical Cancer*
712 *Research* 21: 2305–2314.
713 10. Davol, P. A., J. A. Smith, N. Kouttab, G. J. Elfenbein, and L. G.
714 Lum. 2004. Anti-CD3 × Anti-HER2 Bispecific Antibody Effectively
715 Redirects Armed T Cells to Inhibit Tumor Development and Growth

716 in Hormone-Refractory Prostate Cancer–Bearing Severe Combined
717 Immunodeficient Beige Mice. *Clin Prostate Cancer* 3: 112–121.
718 11. Yankelevich, M., A. Thakur, S. Modak, R. Chu, J. Taub, A.
719 Martin, D. Schalk, A. Schienshang, S. Whitaker, K. Rea, D. W. Lee,
720 Q. Liu, A. F. Shields, N. K. V. Cheung, and L. G. Lum. 2024.
721 Targeting refractory/recurrent neuroblastoma and osteosarcoma with
722 anti-CD3×anti-GD2 bispecific antibody armed T cells. *J Immunother*
723 *Cancer* 12: e008744.
724 12. Lum, L. G., A. Thakur, Z. Al-Kadhimi, G. A. Colvin, F. J.
725 Cummings, R. D. Legare, D. S. Dizon, N. Kouttab, A. Maizel, W.
726 Colaiace, Q. Liu, and R. Rathore. 2015. Targeted T-cell therapy in
727 stage IV breast cancer: A phase i clinical trial. *Clinical Cancer*
728 *Research* 21: 2305–2314.
729 13. Lum, L. G., Z. Al-Kadhimi, A. Deol, V. Kondadasula, D. Schalk,
730 E. Tomashewski, P. Steele, K. Fields, M. Giroux, Q. Liu, L. Flaherty,
731 M. Simon, and A. Thakur. 2021. Phase II clinical trial using anti-CD3
732 × anti-HER2 bispecific antibody armed activated T cells (HER2
733 BATs) consolidation therapy for HER2 negative (0–2+) metastatic
734 breast cancer. *J Immunother Cancer* 9: e002194.
735 14. Rugo, H. S., J. P. Delord, S. A. Im, P. A. Ott, S. A. Piha-Paul, P.
736 L. Bedard, J. Sachdev, C. Le Tourneau, E. M. J. van Brummelen, A.
737 Varga, R. Salgado, S. Loi, S. Saraf, D. Pietrangelo, V. Karantza, and
738 A. R. Tan. 2018. Safety and Antitumor Activity of Pembrolizumab in
739 Patients with Estrogen Receptor-Positive/Human Epidermal Growth
740 Factor Receptor 2-Negative Advanced Breast Cancer. *Clin Cancer*
741 *Res* 24: 2804–2811.
742 15. Cardoso, F., L. Jia, K. Hirshfield, and V. Karantza. 2019.
743 KEYNOTE-756: Randomized, double-blind, phase III study of
744 pembrolizumab vs placebo + neoadjuvant chemotherapy (CT) and
745 adjuvant endocrine therapy (ET) for high-risk, early-stage estrogen
746 receptor–positive human epidermal growth factor receptor 2–negative
747 (ER+/HER2−) breast cancer (BC). *Annals of Oncology* 30: iii38.
748 16. Dirix, L. Y., I. Takacs, G. Jerusalem, P. Nikolinakos, H. T.
749 Arkenau, A. Forero-Torres, R. Boccia, M. E. Lippman, R. Somer, M.
750 Smakal, L. A. Emens, B. Hrinczenko, W. Edenfield, J. Gurtler, A. von
751 Heydebreck, H. J. Grote, K. Chin, and E. P. Hamilton. 2018.
752 Avelumab, an anti-PD-L1 antibody, in patients with locally advanced
753 or metastatic breast cancer: a phase 1b JAVELIN Solid Tumor study.
754 *Breast Cancer Res Treat* 167: 671–686.
755 17. Rotte, A., J. Y. Jin, and V. Lemaire. 2018. Mechanistic overview
756 of immune checkpoints to support the rational design of their
757 combinations in cancer immunotherapy. *Ann Oncol* 29: 71–83.
758 18. Goleva, E., T. Lyubchenko, L. Kraehenbuehl, M. E. Lacouture, D.
759 Y. M. Leung, and J. A. Kern. 2021. Our current understanding of
760 checkpoint inhibitor therapy in cancer immunotherapy. *Ann Allergy*
761 *Asthma Immunol* 126: 630–638.

19. Ildefonso, G. V., and S. D. Finley. 2023. A data-driven Boolean model explains memory subsets and evolution in CD8+ T cell exhaustion. *npj Systems Biology and Applications 2023 9:1* 9: 1–13.
20. Yan, M., J. Hu, H. Yuan, L. Xu, G. Liao, Z. Jiang, J. Zhu, B. Pang, Y. Ping, Y. Zhang, Y. Xiao, and X. Li. 2021. Dynamic regulatory networks of T cell trajectory dissect transcriptional control of T cell state transition. *Mol Ther Nucleic Acids* 26: 1115–1129.
21. Bolouri, H., M. Young, J. Beilke, R. Johnson, B. Fox, L. Huang, C. C. Santini, C. M. Hill, A. R. van der V. de Vries, P. T. Shannon, A. Dervan, P. Sivakumar, M. Trotter, D. Bassett, and A. Ratushny. 2020. Integrative network modeling reveals mechanisms underlying T cell exhaustion. *Scientific Reports 2020 10:1* 10: 1–15.
22. Sontag, E. D. 2017. A Dynamic Model of Immune Responses to Antigen Presentation Predicts Different Regions of Tumor or Pathogen Elimination. *Cell Syst* 4: 231-241.e11.
23. Cess, C. G., and S. D. Finley. 2020. Data-driven analysis of a mechanistic model of CAR T cell signaling predicts effects of cell-to-cell heterogeneity. *J Theor Biol* 489: 110125.
24. Uberti, J. P., I. Joshi, M. Ueda, F. Martilotti, L. L. Sensenbrenner, and L. G. Lum. 1994. Preclinical Studies Using Immobilized OKT3 to Activate Human T Cells for Adoptive Immunotherapy: Optimal Conditions for the Proliferation and Induction of Non-MHC-Restricted Cytotoxicity. *Clin Immunol Immunopathol* 70: 234–240.
25. Sen, M., D. M. Wankowski, N. K. Garlie, R. E. Siebenlistd, D. Van Epps, A. V. LeFever, and L. G. Lum. 2001. Use of anti-CD3 x anti-HER2/neu bispecific antibody for redirecting cytotoxicity of activated T cells toward HER2/neu+ tumors. *J Hematother Stem Cell Res* 10: 247–260.
26. Sen, M., D. M. Wankowski, N. K. Garlie, R. E. Siebenlistd, D. Van Epps, A. V. LeFever, and L. G. Lum. 2004. Use of Anti-CD3 × Anti-HER2/neu Bispecific Antibody for Redirecting Cytotoxicity of Activated T Cells Toward HER2/neu+ Tumors. *https://home.liebertpub.com/scd* 10: 247–260.
27. Stoeckius, M., C. Hafemeister, W. Stephenson, B. Houck-Loomis, P. K. Chattopadhyay, H. Swerdlow, R. Satija, and P. Smibert. 2017. Simultaneous epitope and transcriptome measurement in single cells. *Nature Methods 2017 14:9* 14: 865–868.
28. Hao, Y., T. Stuart, M. H. Kowalski, S. Choudhary, P. Hoffman, A. Hartman, A. Srivastava, G. Molla, S. Madad, C. Fernandez-Granda, and R. Satija. 2023. Dictionary learning for integrative, multimodal and scalable single-cell analysis. *Nature Biotechnology 2023 42:2* 42: 293–304.
29. Thakur, A., J. Ung, E. N. Tomaszewski, A. Schienschang, T. M. LaBrie, D. L. Schalk, and L. G. Lum. 2021. Priming of pancreatic cancer cells with bispecific antibody armed activated T cells sensitizes tumors for enhanced chemoresponsiveness. *Oncoimmunology* 10.

30. Chong, I. G., and C. H. Jun. 2005. Performance of some variable selection methods when multicollinearity is present. *Chemometrics and Intelligent Laboratory Systems* 78: 103–112.
31. Joslyn, L. R., D. E. Kirschner, and J. J. Linderman. CaliPro: A Calibration Protocol That Utilizes Parameter Density Estimation to Explore Parameter Space and Calibrate Complex Biological Models. .
32. Guo, M., M. Y. R. Liu, and D. G. Brooks. 2024. Regulation and impact of tumor-specific CD4+ T cells in cancer and immunotherapy. *Trends Immunol* 45: 303–313.
33. Zheng, L., S. Qin, W. Si, A. Wang, B. Xing, R. Gao, X. Ren, L. Wang, X. Wu, J. Zhang, N. Wu, N. Zhang, H. Zheng, H. Ouyang, K. Chen, Z. Bu, X. Hu, J. Ji, and Z. Zhang. 2021. Pan-cancer single-cell landscape of tumor-infiltrating T cells. *Science (1979)* 374.
34. Correia, M. P., A. Stojanovic, K. Bauer, D. Juraeva, L. O. Tykocinski, H. M. Lorenz, B. Brors, and A. Cerwenka. 2018. Distinct human circulating NKp30+FceRIγ+CD8+ T cell population exhibiting high natural killer-like antitumor potential. *Proc Natl Acad Sci U S A* 115: E5980–E5989.
35. Garner, L. C., A. Amini, M. E. B. FitzPatrick, M. J. Lett, G. F. Hess, M. Filipowicz Sinnreich, N. M. Provine, and P. Klenerman. 2023. Single-cell analysis of human MAIT cell transcriptional, functional and clonal diversity. *Nature Immunology 2023 24:9* 24: 1565–1578.
36. Lu, B., M. Liu, J. Wang, H. Fan, D. Yang, L. Zhang, X. Gu, J. Nie, Z. Chen, A. J. Corbett, M. J. Zhan, S. Zhang, V. L. Bryant, A. M. Lew, J. McCluskey, H. bin Luo, J. Cui, Y. Zhang, Y. Zhan, and G. Lu. 2020. IL-17 production by tissue-resident MAIT cells is locally induced in children with pneumonia. *Mucosal Immunol* 13: 824–835.
37. Intlekofer, A. M., N. Takemoto, E. J. Wherry, S. A. Longworth, J. T. Northrup, V. R. Palanivel, A. C. Mullen, C. R. Gasink, S. M. Kaech, J. D. Miller, L. Gapin, K. Ryan, A. P. Russ, T. Lindsten, J. S. Orange, A. W. Goldrath, R. Ahmed, and S. L. Reiner. 2005. Effector and memory CD8+ T cell fate coupled by T-bet and eomesodermin. *Nature Immunology 2005 6:12* 6: 1236–1244.
38. Willinger, T., T. Freeman, M. Herbert, H. Hasegawa, A. J. McMichael, and M. F. C. Callan. 2006. Human Naive CD8 T Cells Down-Regulate Expression of the WNT Pathway Transcription Factors Lymphoid Enhancer Binding Factor 1 and Transcription Factor 7 (T Cell Factor-1) following Antigen Encounter In Vitro and In Vivo. *The Journal of Immunology* 176: 1439–1446.
39. Khan, O., J. R. Giles, S. McDonald, S. Manne, S. F. Ngiow, K. P. Patel, M. T. Werner, A. C. Huang, K. A. Alexander, J. E. Wu, J. Attanasio, P. Yan, S. M. George, B. Bengsch, R. P. Staupe, G. Donahue, W. Xu, R. K. Amaravadi, X. Xu, G. C. Karakousis, T. C. Mitchell, L. M. Schuchter, J. Kaye, S. L. Berger, and E. J. Wherry.

2019. TOX transcriptionally and epigenetically programs CD8+ T cell exhaustion. *Nature 2019 571:7764* 571: 211–218.
40. Bullock, T. N. 2017. Stimulating CD27 to quantitatively and qualitatively shape adaptive immunity to cancer. *Curr Opin Immunol* 45: 82–88.
41. Albrecht, I., U. Niesner, M. Janke, A. Menning, C. Loddenkemper, A. A. Kühl, I. Lepenies, M. H. Lexberg, K. Westendorf, K. Hradilkova, J. Grün, A. Hamann, J. A. Epstein, H. D. Chang, K. Tokoyoda, and A. Radbruch. 2010. Persistence of effector memory Th1 cells is regulated by Hopx. *Eur J Immunol* 40: 2993–3006.
42. Shehata, H. M., S. Khan, E. Chen, P. E. Fields, R. A. Flavell, and S. Sanjabi. 2018. Lack of Sprouty 1 and 2 enhances survival of effector CD8+ T cells and yields more protective memory cells. *Proc Natl Acad Sci U S A* 115: E8939–E8947.
43. Chen, Y., J. Gao, M. Ma, K. Wang, F. Liu, F. Yang, X. Zou, Z. Cheng, and D. Wu. 2024. The potential role of CMC1 as an immunometabolic checkpoint in T cell immunity. *Oncoimmunology* 13.
44. Thommen, D. S., J. Schreiner, P. Müller, P. Herzig, A. Roller, A. Belousov, P. Umana, P. Pisa, C. Klein, M. Bacac, O. S. Fischer, W. Moersig, S. S. Prince, V. Levitsky, V. Karanikas, D. Lardinois, and A. Zippelius. 2015. Progression of lung cancer is associated with increased dysfunction of T cells defined by coexpression of multiple inhibitory receptors. *Cancer Immunol Res* 3: 1344–1354.
45. Baitsch, L., A. Legat, L. Barba, S. A. Marraco, J. P. Rivals, P. Baumgaertner, C. Christiansen-Jucht, H. Bouzourene, D. Rimoldi, H. Pircher, N. Rufer, M. Matter, O. Michielin, and D. E. Speiser. 2012. Extended Co-Expression of Inhibitory Receptors by Human CD8 T-Cells Depending on Differentiation, Antigen-Specificity and Anatomical Localization. *PLoS One* 7: e30852.
46. Li, X., R. Wang, P. Fan, X. Yao, L. Qin, Y. Peng, M. Ma, N. Asley, X. Chang, Y. Feng, Y. Hu, Y. Zhang, C. Li, G. Fanning, S. Jones, C. Verrill, D. Maldonado-Perez, P. Sopp, C. Waugh, S. Taylor, S. McGowan, V. Cerundolo, C. Conlon, A. McMichael, S. Lu, X. Wang, N. Li, and T. Dong. 2019. A comprehensive analysis of key immune checkpoint receptors on tumor-infiltrating t cells from multiple types of cancer. *Front Oncol* 9: 472080.
47. Chiang, E. Y., and I. Mellman. 2022. TIGIT-CD226-PVR axis: advancing immune checkpoint blockade for cancer immunotherapy. *J Immunother Cancer* 10: e004711.
48. Boissière-Michot, F., M. C. Chateau, S. Thézenas, S. Guiu, A. Bobrie, and W. Jacot. 2022. Correlation of the TIGIT-PVR immune checkpoint axis with clinicopathological features in triple-negative breast cancer. *Front Immunol* 13: 1058424.

49. Worboys, J. D., K. N. Vowell, R. K. Hare, A. R. Ambrose, M. Bertuzzi, M. A. Conner, F. P. Patel, W. H. Zammit, J. Gali-Moya, K. S. Hazime, K. L. Jones, C. Rey, S. Jonjic, T. L. Rovis, G. M. Tannahill, G. D. S. Cruz De Matos, J. D. Waight, and D. M. Davis. 2023. TIGIT can inhibit T cell activation via ligation-induced nanoclusters, independent of CD226 co-stimulation. *Nature Communications 2023 14:1* 14: 1–21.
50. Liu, Z., H. Zeng, K. Jin, Y. Yu, R. You, H. Zhang, C. Liu, X. Su, S. Yan, Y. Chang, L. Liu, L. Xu, J. Xu, Y. Zhu, and Z. Wang. 2022. TIGIT and PD-1 expression atlas predicts response to adjuvant chemotherapy and PD-L1 blockade in muscle-invasive bladder cancer. *British Journal of Cancer 2022 126:9* 126: 1310–1317.
51. Wherry, E. J., and M. Kurachi. 2015. Molecular and cellular insights into T cell exhaustion. *Nature Reviews Immunology 2015 15:8* 15: 486–499.
52. Takamatsu, K., N. Tanaka, K. Hakozaki, R. Takahashi, Y. Teranishi, T. Murakami, R. Kufukihara, N. Niwa, S. Mikami, T. Shinojima, T. Sasaki, Y. Sato, H. Kume, S. Ogawa, K. Kakimi, T. Kamatani, F. Miya, T. Tsunoda, E. Aimono, H. Nishihara, K. Sawada, T. Imamura, R. Mizuno, and M. Oya. 2021. Profiling the inhibitory receptors LAG-3, TIM-3, and TIGIT in renal cell carcinoma reveals malignancy. *Nature Communications 2021 12:1* 12: 1–12.
53. Workman, C. J., and D. A. A. Vignali. 2003. The CD4-related molecule, LAG-3 (CD223), regulates the expansion of activated T cells. *Eur J Immunol* 33: 970–979.
54. Grosso, J. F., M. V. Goldberg, D. Getnet, T. C. Bruno, H.-R. Yen, K. J. Pyle, E. Hipkiss, D. A. A. Vignali, D. M. Pardoll, and C. G. Drake. 2009. Functionally Distinct LAG-3 and PD-1 Subsets on Activated and Chronically Stimulated CD8 T Cells. *The Journal of Immunology* 182: 6659–6669.
55. Kallies, A., D. Zehn, and D. T. Utzschneider. 2019. Precursor exhausted T cells: key to successful immunotherapy? *Nature Reviews Immunology 2019 20:2* 20: 128–136.
56. Ngiow, S. F., S. Manne, Y. J. Huang, T. Azar, Z. Chen, D. Mathew, Q. Chen, O. Khan, J. E. Wu, V. Alcalde, A. J. Flowers, S. McClain, A. E. Baxter, M. Kurachi, J. Shi, A. C. Huang, J. R. Giles, A. H. Sharpe, D. A. A. Vignali, and E. J. Wherry. 2024. LAG-3 sustains TOX expression and regulates the CD94/NKG2-Qa-1b axis to govern exhausted CD8 T cell NK receptor expression and cytotoxicity. *Cell* 187: 4336-4354.e19.
57. Andrews, L. P., S. C. Butler, J. Cui, A. R. Cillo, C. Cardello, C. Liu, E. A. Brunazzi, A. Baessler, B. Xie, S. R. Kunning, S. F. Ngiow, Y. J. Huang, S. Manne, A. H. Sharpe, G. M. Delgoffe, E. J. Wherry, J. M. Kirkwood, T. C. Bruno, C. J. Workman, and D. A. A. Vignali. 2024. LAG-3 and PD-1 synergize on CD8+ T cells to drive T cell

exhaustion and hinder autocrine IFN-γ-dependent anti-tumor immunity. *Cell* 187: 4355-4372.e22.

58. Baixeras, E., B. Huard, C. Miossec, S. Jitsukawa, M. Martin, T. Hercend, C. Auffray, F. Triebel, and D. Piatier-Tonneau. 1992. Characterization of the lymphocyte activation gene 3-encoded protein. A new ligand for human leukocyte antigen class II antigens. *Journal of Experimental Medicine* 176: 327–337.

59. Williams, C. B., E. S. Yeh, and A. C. Soloff. 2016. Tumor-associated macrophages: unwitting accomplices in breast cancer malignancy. *npj Breast Cancer 2016 2:1* 2: 1–12.

60. Medrek, C., F. Pontén, K. Jirström, and K. Leandersson. 2012. The presence of tumor associated macrophages in tumor stroma as a prognostic marker for breast cancer patients. *BMC Cancer* 12: 1–9.

61. Guy, C., D. M. Mitrea, P. C. Chou, J. Temirov, K. M. Vignali, X. Liu, H. Zhang, R. Kriwacki, M. P. Bruchez, S. C. Watkins, C. J. Workman, and D. A. A. Vignali. 2022. LAG3 associates with TCR–CD3 complexes and suppresses signaling by driving co-receptor–Lck dissociation. *Nature Immunology 2022 23:5* 23: 757–767.

62. Bachmann, M. F., M. Barner, A. Viola, and M. Kopf. Distinct kinetics of cytokine production and cytolysis in effector and memory T cells after viral infection. .

63. Veiga-Fernandes, H., U. Walter, C. Bourgeois, A. McLean, and B. Rocha. 2000. Response of naïve and memory CD8+ T cells to antigen stimulation in vivo. *Nature Immunology 2000 1:1* 1: 47–53.

64. Helmich, B. K., and R. W. Dutton. 2001. The role of adoptively transferred CD8 T cells and host cells in the control of the growth of the EG7 thymoma: factors that determine the relative effectiveness and homing properties of Tc1 and Tc2 effectors. *J Immunol* 166: 6500–6508.

65. Dong, C. 2021. Cytokine Regulation and Function in T Cells. *Annu Rev Immunol* 39: 51–76.

66. Sumida, T. S., S. Dulberg, J. C. Schupp, M. R. Lincoln, H. A. Stillwell, P. P. Axisa, M. Comi, A. Unterman, N. Kaminski, A. Madi, V. K. Kuchroo, and D. A. Hafler. 2022. Type I interferon transcriptional network regulates expression of coinhibitory receptors in human T cells. *Nature Immunology 2022 23:4* 23: 632–642.

67. Spranger, S., R. M. Spaapen, Y. Zha, J. Williams, Y. Meng, T. T. Ha, and T. F. Gajewski. 2013. Up-regulation of PD-L1, IDO, and Tregs in the melanoma tumor microenvironment is driven by CD8+ T cells. *Sci Transl Med* 5.

68. Sato, H., A. Niimi, T. Yasuhara, T. B. M. Permata, Y. Hagiwara, M. Isono, E. Nuryadi, R. Sekine, T. Oike, S. Kakoti, Y. Yoshimoto, K. D. Held, Y. Suzuki, K. Kono, K. Miyagawa, T. Nakano, and A. Shibata. 2017. DNA double-strand break repair pathway regulates PD-L1 expression in cancer cells. *Nature Communications 2017 8:1* 8: 1–11.

69. Strickland, K. C., B. E. Howitt, S. A. Shukla, S. Rodig, L. L. Ritterhouse, J. F. Liu, J. E. Garber, D. Chowdhury, C. J. Wu, A. D. D'Andrea, U. A. Matulonis, and P. A. Konstantinopoulos. 2016. Association and prognostic significance of BRCA1/2-mutation status with neoantigen load, number of tumor-infiltrating lymphocytes and expression of PD-1/PD-L1 in high grade serous ovarian cancer. *Oncotarget* 7: 13587.

70. Rosenbaum, M. W., J. R. Bledsoe, V. Morales-Oyarvide, T. G. Huynh, and M. Mino-Kenudson. 2016. PD-L1 expression in colorectal cancer is associated with microsatellite instability, BRAF mutation, medullary morphology and cytotoxic tumor-infiltrating lymphocytes. *Modern Pathology* 29: 1104–1112.

71. Gorvel, L., and D. Olive. 2020. Targeting the "PVR–TIGIT axis" with immune checkpoint therapies. *F1000Res* 9.

72. Messenheimer, D. J., S. M. Jensen, M. E. Afentoulis, K. W. Wegmann, Z. Feng, D. J. Friedman, M. J. Gough, W. J. Urba, and B. A. Fox. Cancer Therapy: Preclinical Timing of PD-1 Blockade Is Critical to Effective Combination Immunotherapy with Anti-OX40. *Clin Cancer Res* 23.

73. Koyama, S., E. A. Akbay, Y. Y. Li, G. S. Herter-Sprie, K. A. Buczkowski, W. G. Richards, L. Gandhi, A. J. Redig, S. J. Rodig, H. Asahina, R. E. Jones, M. M. Kulkarni, M. Kuraguchi, S. Palakurthi, P. E. Fecci, B. E. Johnson, P. A. Janne, J. A. Engelman, S. P. Gangadharan, D. B. Costa, G. J. Freeman, R. Bueno, F. S. Hodi, G. Dranoff, K. K. Wong, and P. S. Hammerman. 2016. Adaptive resistance to therapeutic PD-1 blockade is associated with upregulation of alternative immune checkpoints. *Nature Communications 2016 7:1* 7: 1–9.

74. Cho, E., R. Singh, C. Han, S. H. Kim, K. H. Kim, B. M. Park, D. H. Shin, S. Han, Y. H. Kim, B. S. Kwon, K. T. Nam, and B. K. Choi. 2023. 4-1BB-4-1BBL cis-interaction contributes to the survival of self-reactive CD8+ T cell. *Cellular & Molecular Immunology 2023 20:9* 20: 1077–1080.

75. Vaishampayan, U. N., A. Thakur, W. Chen, A. Deol, M. Patel, K. Dobson, B. Dickow, D. Schalk, A. Schienschang, S. Whitaker, A. Polend, J. A. Fontana, E. I. Heath, and L. G. Lum. 2023. Phase II Trial of Pembrolizumab and Anti-CD3 x Anti-HER2 Bispecific Antibody-Armed Activated T Cells in Metastatic Castration-Resistant Prostate Cancer. *Clinical Cancer Research* 29: 122–133.

Figure captions

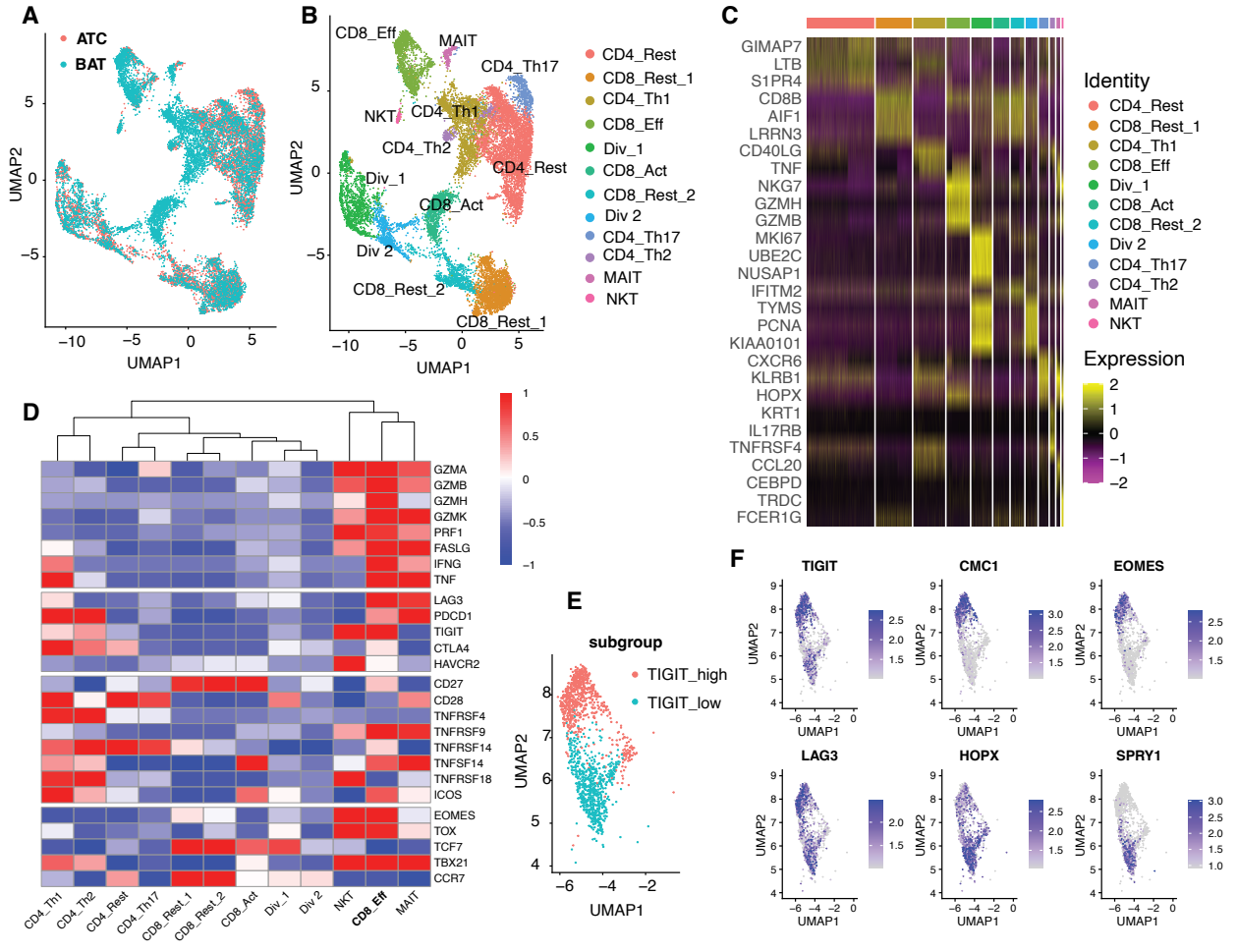

Figure 1:

A: UMAP plot of CITE-seq data labeled by bispecific antibody arming. ATC: unarmed Activated T Cells, BAT: Bispecific antibody-armed Activated T cells

B: A UMAP plot of T cells clustered by similarity in gene expression. Labels were chosen based on expression of significantly upregulated marker genes. CD4_Rest = Resting CD4 T cells; CD8_Rest_1 = Group 1 Resting CD8 T cells; CD4_Th1 = Th1 CD4 T cells; CD8_Eff = Effector CD8 T cells; Div_1 = Group 1 Dividing T cells; CD8_Act = Activated CD8 T cells; CD8_Rest_2 = Group 2 Resting CD8 T cells; Div_2 = Group 2 Dividing T cells; CD4_Th17 = Th17 CD4 T cells; CD4_Th2 = Th2 CD4 T cells; MAIT = Mucosal Associated Invariant T cells; NKT = NK-like T cells

1041 C: Heatmap of most differentially expressed genes as determined by a Wilcoxon ranked sum test.
1042 Genes shown most strongly differentiate each group from all other groups and were used to
1043 determine the labels in 1B.
1044 D: A heat map of average gene expression scaled across groups. Genes displayed are involved
1045 in cytotoxicity (top), T cell inhibition (second top), T cell costimulation (second bottom), and T cell
1046 maturation and differentiation (bottom).
1047 E: A re-clustered UMAP of effector CD8 T cells.
1048 F: Differentially expressed genes between the two CD8_Eff clusters.
1049

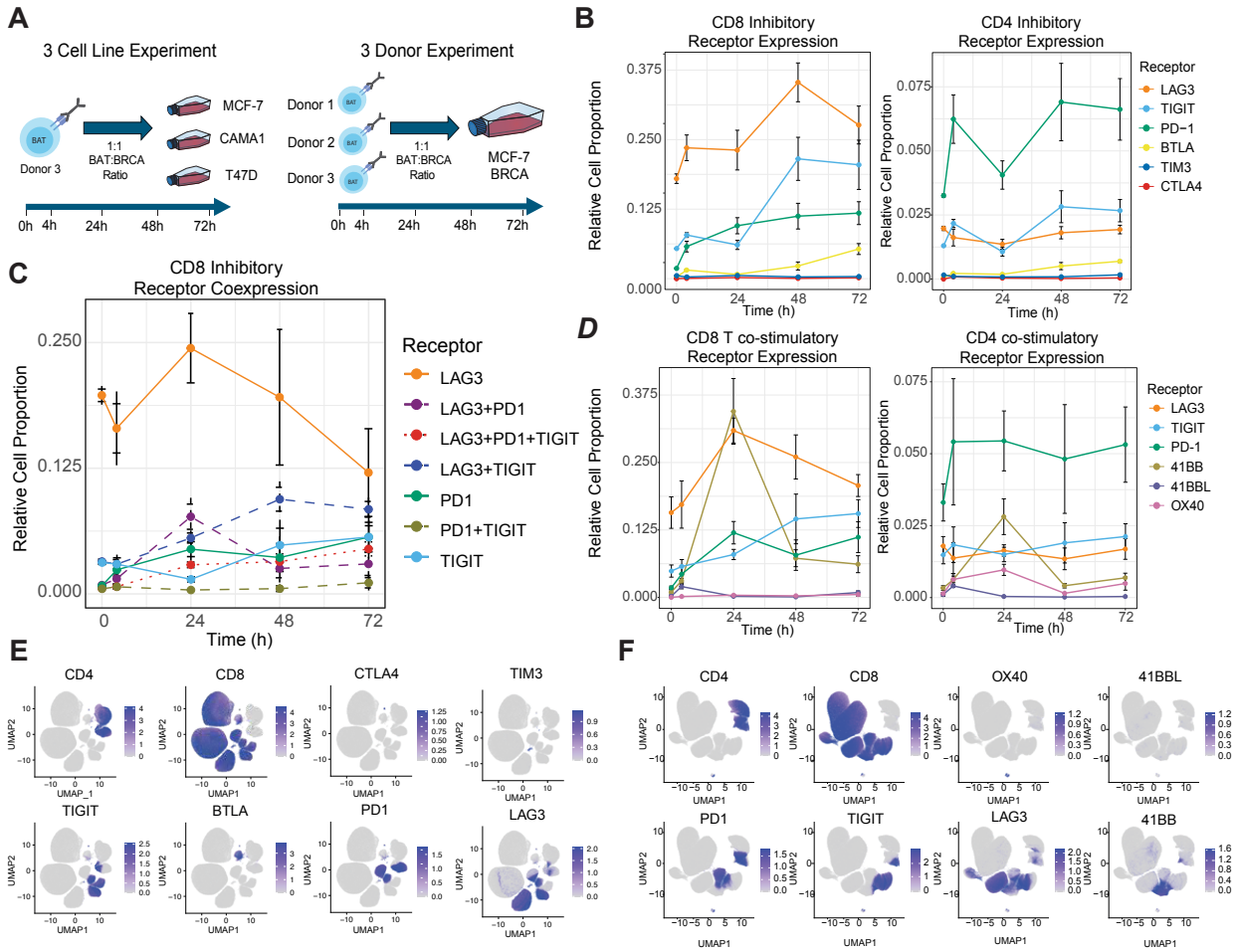

Figure 2:

A: Diagram illustrating the setup and data collection for the two sets of flow cytometry experiments performed. Left Panel - BATs generated from Donor 1 challenged against MCF-7, CAMA1, and T47D breast cancer cell lines. Samples collected at 0, 4, 24, 48, and 72 hours and designated '3 Cell Line Experiment'. Right Panel - BATs generated from Donors 1, 2, and 3 challenged separately against MCF-7 breast cancer cell line. Samples collected at 0, 4, 24, 48, and 72 hours and designated '3 Donor Experiment'.

B: Inhibitory panel receptor expression on CD8 (left panel) and CD4 (right panel) BATs. Data shown was collected from the 3 Cell Line experiment and is presented as the mean value across

1061 all cell lines. Error bars indicate standard error within each data group. Each line represents the
1062 relative proportion of the cells that express a marker regardless of other marker expression.
1063 C: Relative cell proportion of CD8 cells expressing LAG3, TIGIT, PD-1, or a combination thereof.
1064 Cells were binned specificly by their expression or combination of expression of LAG3, TIGIT,
1065 and PD-1. Unlike Panels B and D, there is no overlap between groups containing a common
1066 ligand. For example, the TIGIT+ CD8 T cell subset does not express PD-1 or LAG3. Samples
1067 collected at 0, 4, 24,48, and 72 hours. Data represents mean value across 3 Cell Line experiment
1068 as collected in the coexpression panel. Error bars represent the range within each sample
1069 timepoint.
1070 D: Coexpression panel receptor expression on CD8 (left panel) and CD4 (right panel) BATs. Data
1071 shown was collected from the 3 Cell Line experiment and is presented as the mean value across
1072 all cell lines. Error bars indicate standard error within each data group. Each line represents the
1073 relative proportion of the cells that express a marker and can have other markers simultaneously
1074 expressed.
1075 E: UMAP of BAT cells from the 3 Cell Line experiment clustered by receptor expression as
1076 measured by flow cytometry in the inhibitory panel.
1077 F: UMAP of BAT cells from the Cell Line experiment clustered by receptor expression as
1078 measured by flow cytometry in the coexpression panel.
1079

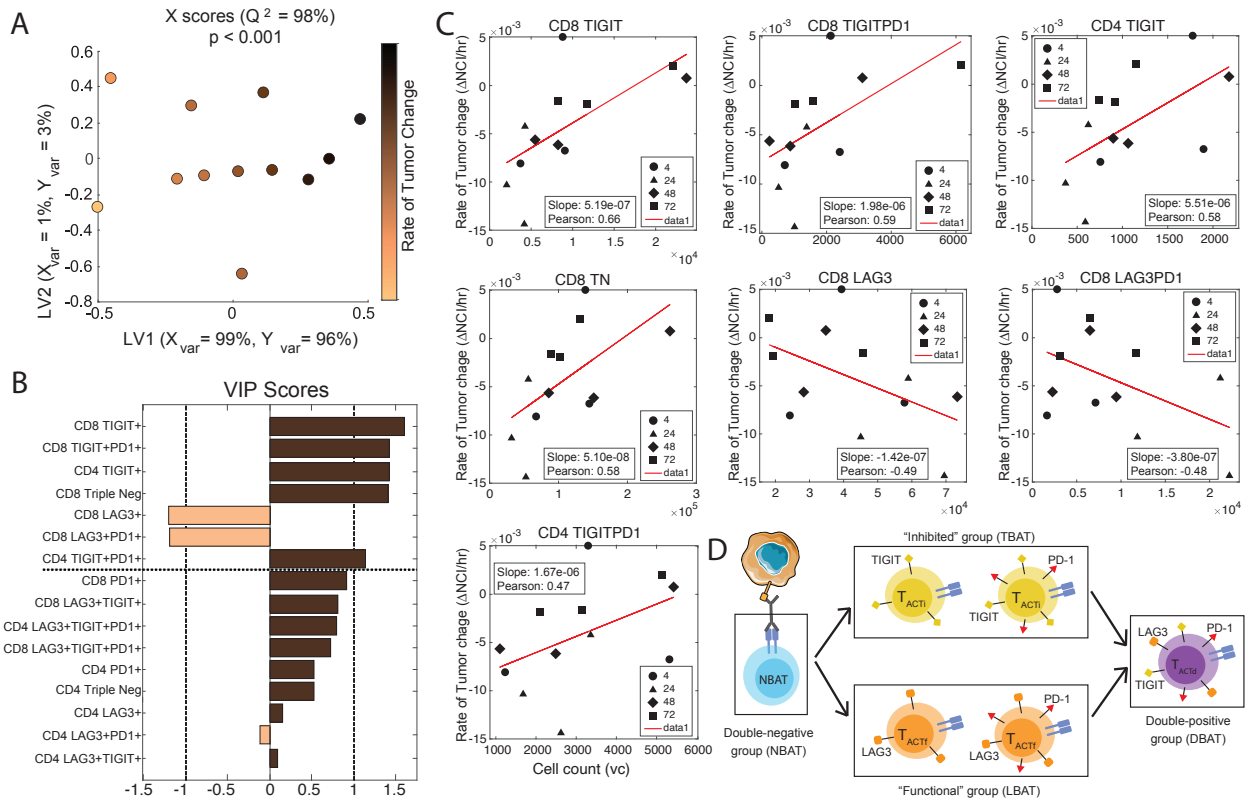

Figure 3:

A: OPLS-R model of rate of tumor change predicted by BAT subpopulations from the 3 Cell Line experiment. BATs were binned by CD4 or CD8 expression, and further binned by expression of LAG3, TIGIT, and/or PD-1. Cells expressing more than one receptor were binned in separate categories, with cells expressing all three receptors being designated tri-positive (TP). BATs lacking receptors were designated tri-negative (TN).

B: VIP scores generated by PLS-R model in Figure 3A. Subpopulation impact is designated by the magnitude of the VIP score, with scores of magnitude >1 designated as greater-than-average contribution of that cell subpopulation to tumor reduction. Subpopulations with scores colored tan are associated with reduced rate of tumor change, while subpopulations with scores colored brown are negatively associated with reduced rate of tumor change.

C: Scatter plots comparing the viable cell count of BAT subpopulations (x-axis) to rate of tumor change (y-axis) for subpopulations with VIP scores >1. NCI = normalized cell index.

D: Diagram of BAT developmental progression as assumed by the model. BATs are grouped as NBATs (LAG3-/TIGIT-), LBATs (LAG3+/TIGIT-), TBATs (LAG3-/TIGIT+), or DBATs (LAG3+/TIGIT+). PD-1 expression does not factor into grouping and can be present within any group. These four groups are used to govern tumor reduction in the models presented in Figures 4 and 5.

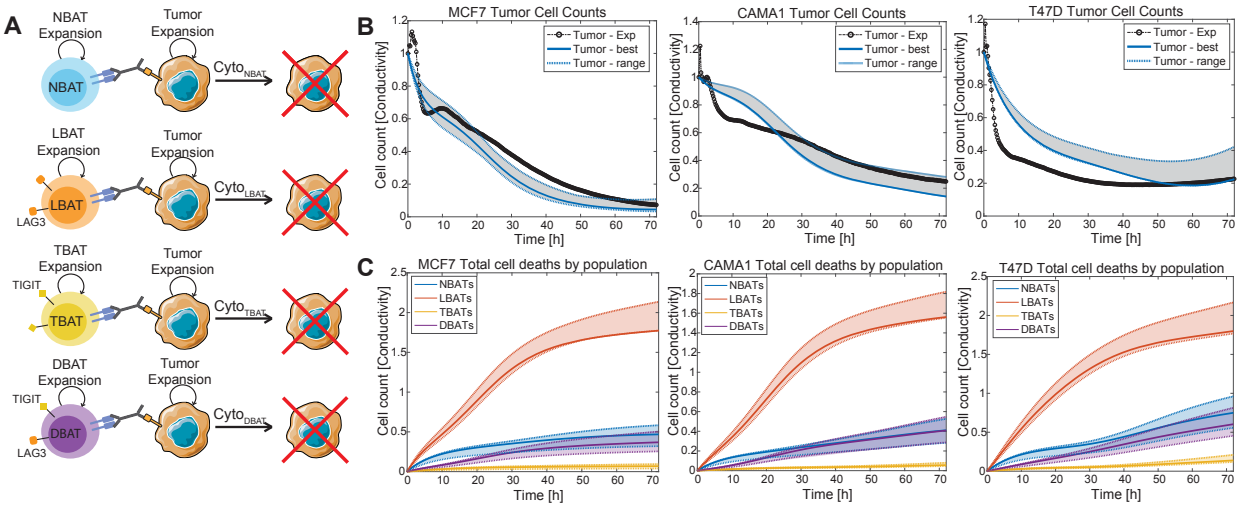

Figure 4:

A: Diagram representing processes represented in the model. Tumor expansion parameters were determined by fitting a sigmoidal curve to tumor growth data from control conditions in which BATs were absent. BAT subgroup expansion was fit to individual splines to capture the count data determined from flow cytometry. CaliPro was used to fit cytotoxicity rates for each BAT subgroup to match the experimentally measured BAT and tumor cell counts. Data from the 3 Cancer experiment was used in parameter determination and is shown in B and C.

B: MCF-7 (left), CAMA1 (center), and T47D (right) cell counts as measured by RTCA (black) and as predicted by the model (blue). Optimal model prediction in sold blue line, while range of predictions depicted by dotted blue lines.

1111 C: MCF-7 (left), CAMA1 (center), and T47D (right) cell reduction by BAT phenotype as predicted
1112 by the model. LBAT (orange), NBAT (blue), TBAT (yellow), and DBAT (purple) cumulative
1113 reduction is shown for optimal conditions (solid line) and for total range of predictions (dotted
1114 lines).
1115

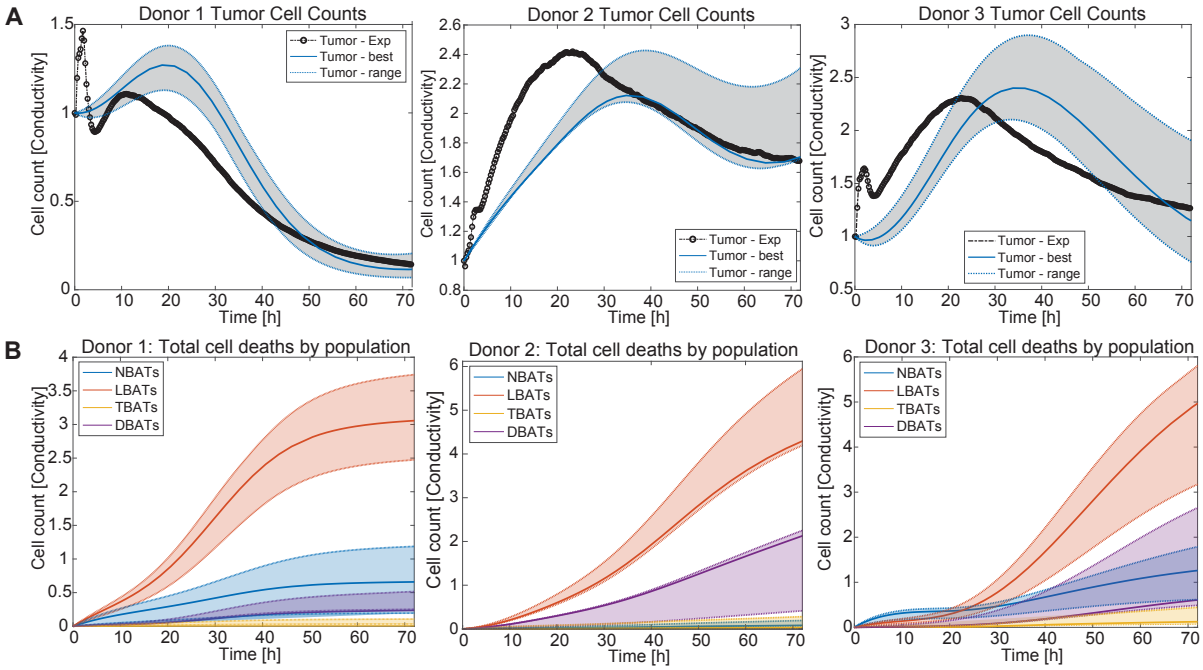

1116

1117 **Figure 5:**

1118 A: MCF-7 cell counts as measured by RTCA (black) and as predicted by the model (blue) when
1119 challenged by Donor 1 (left), Donor 2 (middle), and Donor 3 (right) BATs. Optimal model prediction
1120 in sold blue line, while range of predictions depicted by dotted blue lines.

1121 B: MCF-7 cell reduction by BAT phenotype as predicted by the model when challenged by Donor
1122 1 (left), Donor 2 (middle), and Donor 3 (right) BATs. LBAT (orange), NBAT (blue), TBAT (yellow),
1123 and DBAT (purple) cumulative reduction is shown for optimal conditions (solid line) and for total
1124 range of predictions (dotted lines).
1125